Cell

Clp-targeting BacPROTACs impair mycobacterial proteostasis and survival

Graphical abstract

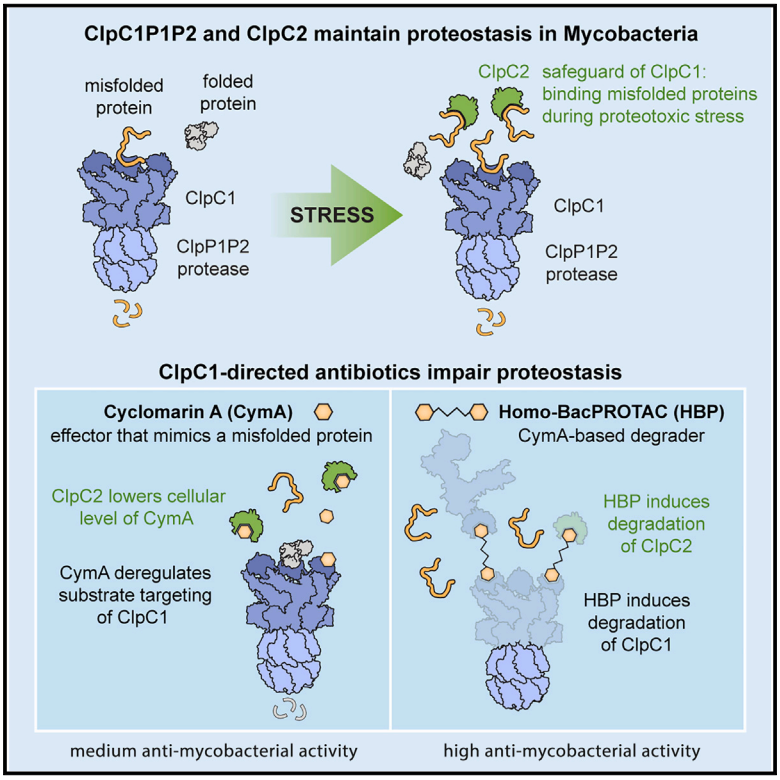

Highlights

- Cyclomarin A and ecumicin hijack ClpC1P1P2 proteases by mimicking damaged proteins
- ClpC2 and ClpC3 function as isolated receptor proteins safeguarding the Clp protease
- Homo-BacPROTACs induce degradation of the essential ClpC1 and its ClpC2 security
- BacPROTACs present potent antibiotics that efficiently kill *M. tuberculosis*

Authors

David M. Hoi, Sabryna Junker, Lukas Junk, ..., Uli Kazmaier, Rainer Kalscheuer, Tim Clausen

Correspondence

lukas.junk@helmholtz-hips.de (L.J.), tim.clausen@imp.ac.at (T.C.)

In brief

Homo-dimeric BacPROTACs induce the self-degradation of essential Clp components of the mycobacterial proteostasis system, introducing a potent antibiotic strategy against *M. tuberculosis*.

Hoi et al., 2023, Cell *186*, 2176–2192
May 11, 2023
https://doi.org/10.1016/j.cell.2023.04.009

CellPress

CellPress
OPEN ACCESS

Cell

Article

Clp-targeting BacPROTACs impair mycobacterial proteostasis and survival

David M. Hoi,[1,9,11,12,13] Sabryna Junker,[1,13] Lukas Junk,[2,3,*] Kristin Schwechel,[4] Katharina Fischel,[5] David Podlesainski,[6] Paige M.E. Hawkins,[7,8] Lasse van Geelen,[4] Farnusch Kaschani,[6] Julia Leodolter,[1] Francesca Ester Morreale,[1] Stefan Kleine,[6] Somraj Guha,[2] Klaus Rumpel,[5] Volker M. Schmiedel,[5] Harald Weinstabl,[5] Anton Meinhart,[1] Richard J. Payne,[7,8] Markus Kaiser,[6] Markus Hartl,[9,12] Guido Boehmelt,[5] Uli Kazmaier,[2,3] Rainer Kalscheuer,[4] and Tim Clausen[1,10,14,*]

[1]Research Institute of Molecular Pathology, Vienna BioCenter, 1030 Vienna, Austria
[2]Saarland University, Organic Chemistry I, 66123 Saarbrücken, Germany
[3]Helmholtz Institute for Pharmaceutical Research Saarland (HIPS), Helmholtz Centre for Infection Research (HZI), 66123 Saarbrücken, Germany
[4]Institute of Pharmaceutical Biology and Biotechnology, Heinrich Heine University, 40225 Düsseldorf, Germany
[5]Boehringer Ingelheim RCV GmbH & Co KG, 1120 Vienna, Austria
[6]University of Duisburg-Essen, Center of Medical Biotechnology, Faculty of Biology, 45141 Essen, Germany
[7]School of Chemistry, University of Sydney, Sydney, NSW 2006, Australia
[8]Australian Research Council Centre of Excellence for Innovations in Peptide and Protein Science, The University of Sydney, NSW 2006, Australia
[9]Max Perutz Labs, Vienna BioCenter, 1030 Vienna, Austria
[10]Medical University of Vienna, 1030 Vienna, Austria
[11]Vienna BioCenter PhD Program, Doctoral School of the University of Vienna and Medical University of Vienna, 1030 Vienna, Austria
[12]University of Vienna, Center for Molecular Biology, Department for Biochemistry and Cell Biology, 1030 Vienna, Austria
[13]These authors contributed equally
[14]Lead contact
*Correspondence: lukas.junk@helmholtz-hips.de (L.J.), tim.clausen@imp.ac.at (T.C.)
https://doi.org/10.1016/j.cell.2023.04.009

SUMMARY

The ClpC1:ClpP1P2 protease is a core component of the proteostasis system in mycobacteria. To improve the efficacy of antitubercular agents targeting the Clp protease, we characterized the mechanism of the antibiotics cyclomarin A and ecumicin. Quantitative proteomics revealed that the antibiotics cause massive proteome imbalances, including upregulation of two unannotated yet conserved stress response factors, ClpC2 and ClpC3. These proteins likely protect the Clp protease from excessive amounts of misfolded proteins or from cyclomarin A, which we show to mimic damaged proteins. To overcome the Clp security system, we developed a BacPROTAC that induces degradation of ClpC1 together with its ClpC2 caretaker. The dual Clp degrader, built from linked cyclomarin A heads, was highly efficient in killing pathogenic *Mycobacterium tuberculosis*, with >100-fold increased potency over the parent antibiotic. Together, our data reveal Clp scavenger proteins as important proteostasis safeguards and highlight the potential of BacPROTACs as future antibiotics.

INTRODUCTION

The overuse of common antibiotics that target protein and nucleic acid synthesis and cell wall assembly has led to the development of pathogenic bacteria harboring multidrug resistance.[1,2] Among these, the extensively drug resistant (XDR) and totally drug resistant (TDR) strains of *Mycobacterium tuberculosis* (*Mtb*) are considered to be highly threatening microbial pathogens,[3,4] which contribute to tuberculosis (TB) constituting the leading global cause of death by bacterial infection. Given the rise of TB infections as a growing and underrecognized threat during the COVID-19 pandemic, the development of further novel antitubercular strategies is urgently needed.[5–7]

One of the most promising *Mtb* drug targets is the ClpC1:ClpP1:ClpP2 (ClpC1P1P2) protease, the mycobacterial equivalent of the eukaryotic proteasome. The Clp proteolytic complex is composed of the AAA (ATPase associated with diverse cellular activities) unfoldase ClpC1 that associates with the ClpP1P2 protease to form a caged degradation chamber. Similar to other Clp proteases, ClpC1 recognizes specific peptide stretches, or degrons, using loops at the entrance of its AAA hexameric ring, whereas the N-terminal domain ($ClpC1_{NTD}$) located on top of the protease functions as a receptor for a separate class of client proteins[8–10] (Figure 1A). Substrates captured by ClpC1 are threaded by ATP-driven power strokes through the pore of the AAA hexamer and translocated into the ClpP1P2 protease chamber for degradation.[11,12]

The ClpC1P1P2 protease is an attractive target for antimicrobial agents due to its essential role in maintaining protein homeostasis and counteracting host-induced stresses, thus making it

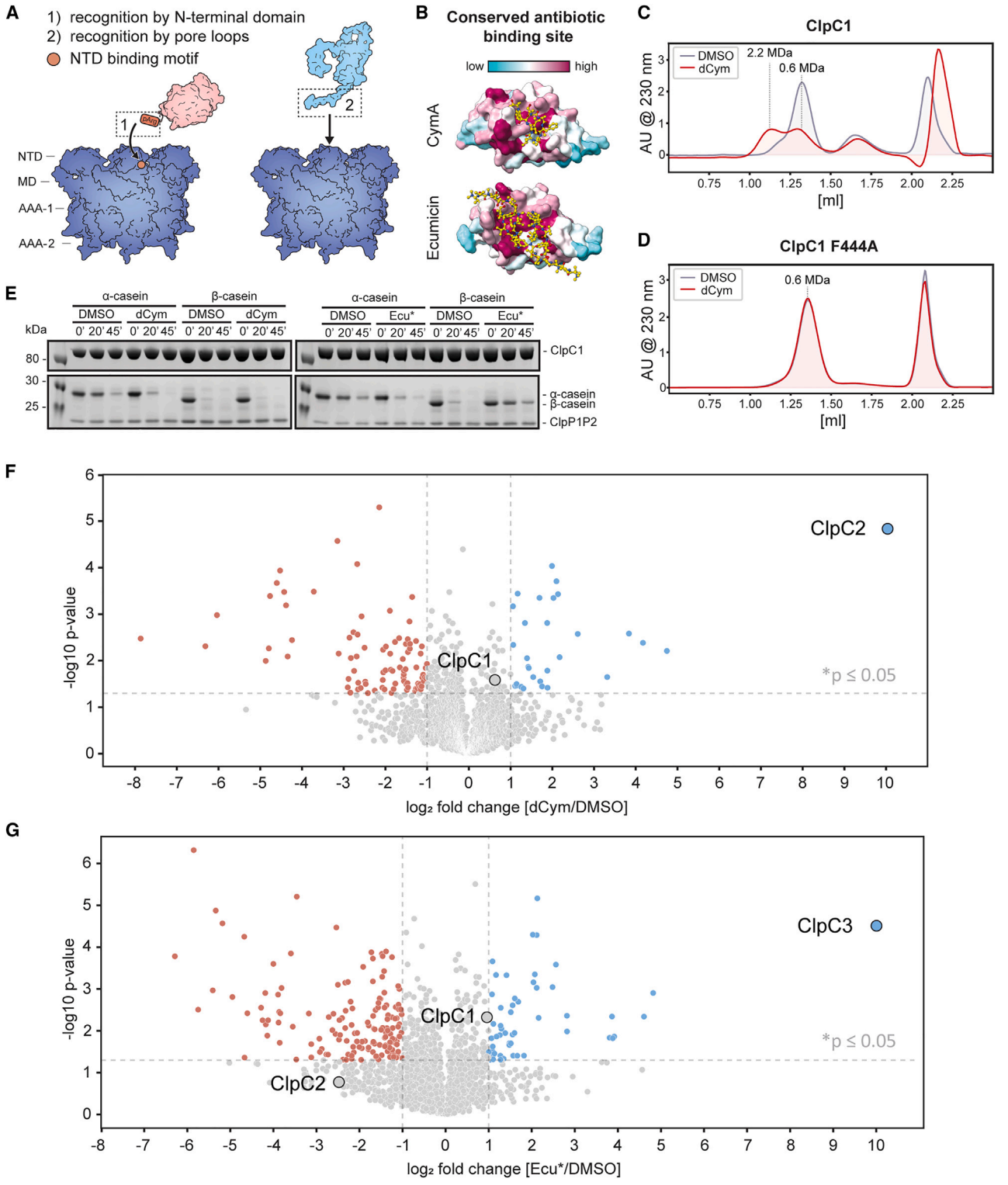

Figure 1. Antitubercular compounds deregulate ClpC1

(A) Substrate recognition by mycobacterial ClpC1 proceeds via specific degrons recognized by the $ClpC1_{NTD}$ or via unfolded protein segments bound by pore loops in the channel formed by the AAA+ ATPase.

(B) $ClpC1_{NTD}$ hydrophobic pocket targeted by antibacterial compounds (upper panel: complex with cyclomarin A, PDB 3WDC; lower panel: complex with ecumicin, PDB 6PBS) is highly conserved, as indicated by the mapped conservation score.

(legend continued on next page)

essential for the full pathogenic potential of mycobacteria.[11,13] Indeed, the Clp protease was identified as a promising mycobacterial target in screening campaigns for lead compounds against alternative drug targets.[14–18] Several antimicrobial agents that target ClpP1P2 or ClpC1 showed antitubercular effects, including efficacy against *Mtb* in human macrophages.[14,18,19] Among the Clp protease targeting antibiotics, acyldepsipeptides are best characterized and interfere with ClpP1P2 by preventing binding of regulatory Clp components.[20–22] Effectors targeting ClpC1 include various natural products such as cyclomarin A, ecumicin, lassomycin and rufomycin.[14,15,18,19,23–25] These cyclic peptides bind to overlapping sites on $ClpC1_{NTD}$ but intriguingly impair ClpC1 activity by seemingly diverse mechanisms. Cyclomarin derived compounds were also recently used to develop small-molecule degraders, called BacPROTACs, that enable ClpC1P1P2-mediated elimination of specific target proteins in mycobacteria.[26]

The antibiotic-binding site on the $ClpC1_{NTD}$ is strongly conserved (Figure 1B), pointing to an important, yet unknown biological function. Given that they bind to the substrate receptor of the Clp protease, we hypothesized that ClpC1-directed antibiotics may induce gross alterations in the Clp degradome of mycobacteria. We thus explored the effect of cyclomarin A and ecumicin on the mycobacterial proteome using quantitative proteomics. In addition to global dysregulation of the proteome at bactericidal concentrations, these data identified two small proteins, which we refer to as ClpC2 and ClpC3, as regulatory components of the mycobacterial Clp degradation system. Using the same ligand-binding sites as those present in ClpC1, the identified Clp proteins compete for substrate binding. Moreover, the two regulatory proteins can sequester ClpC1-directed antibiotics, thus reducing their cytotoxicity. In an effort to overcome ClpC2/ClpC3-mediated protection and efficiently target the Clp degradation machinery as an antibacterial strategy, we synthesized cyclomarin A dimers. These Homo-BacPROTACs (HBPs) were able to direct ClpC1 against itself, inducing its elimination by the ClpC1P1P2 protease, as well as promoting degradation of ClpC2. The HBP degraders exhibited potent killing activity toward *Mtb* in cell culture. Aside from identifying two safeguarding components in the mycobacterial protein quality control (PQC) system, our data highlight the potential of BacPROTACs as antibiotics, allowing us to simultaneously target multiple components of an essential stress response system.

RESULTS

ClpC1-targeting antibiotics imbalance the mycobacterial proteome and induce the expression of small Clp proteins

The most studied natural antibiotics directed against ClpC1 are cyclomarin A and ecumicin[14,18,19] (Figures S1A and S1B). While these two cyclic peptides bind to overlapping $ClpC1_{NTD}$ receptor sites and stimulate ClpC1 ATPase activity to similar degrees, their mode of action differs.[14,18,27] Whereas ClpC1P1P2-mediated degradation has been shown to be enhanced by cyclomarin A, ecumicin instead has been proposed to uncouple the activities of ClpC1 and ClpP1P2, thus reducing protease efficiency. However, the molecular basis underlying their distinct activities is unclear. Likewise, it is not yet known whether and how the deregulation of ClpC1P1P2 may imbalance the mycobacterial proteome. To address these points, we used a recently described ecumicin derivative (Ecu*) (Figure S1B) that exhibits superior antibiotic potency against *Mtb* compared with the parent natural product.[19] As a mimic of the natural cyclomarin A, we used the slightly simplified cyclic peptide desoxycyclomarin C (dCym), which can be produced by chemical total synthesis (Figure S1A).[28,29]

To analyze the molecular basis of ClpC1 deregulation, we reconstituted the interaction of the unfoldase with dCym and Ecu* *in vitro*. As revealed by size-exclusion chromatography (SEC), addition of the antibiotics induced conversion of the ClpC1 hexamer into higher-order oligomers spanning a broad mass range of 0.6–2.2 MDa, as estimated by SEC (Figure 1C). Analysis of the induced peak fraction by negative-stained EM revealed the formation of irregular ClpC1 clusters when incubated with dCym, consisting of 2–4 hexameric particles (Figure S1C). These data are consistent with a recent report showing that cyclomarin A treatment stabilizes higher-order ClpC1 oligomers that have an elevated unfoldase activity.[30] Similar to dCym, we observed that addition of Ecu* resulted in clustering of ClpC1 hexamers (Figure S1D). Together, these data mirror findings in *Bacillus subtilis*, in which ClpC also assembles tetramers of hexamers upon ligand binding to the $ClpC_{NTD}$[26,27] pointing to a broadly conserved mechanism of ClpC regulation. The higher-order complexes are stabilized by contacts between coiled-coil domains (MD) protruding from adjacent hexamers. Aside from promoting oligomer conversion, rearrangement of MD domains destabilizes the auto-inhibited state and induces ATPase activity, thus stimulating unfoldase function.[19,26,27,30] To test whether this activation mechanism is hijacked by dCym, we introduced a site-specific mutation, F444A, a residue at the tip of the ClpC1 MD that is predicted to engage in MD:MD* contacts. Negative-stained EM and SEC analysis confirmed that the F444A mutation abolishes dCym-induced oligomer conversion (Figures 1D and S1E). These data show that dCym binding to ClpC1 induces reorientation of MD coiled-coils thereby transforming the latent hexamer into active higher-order complexes.

To test the effect of ClpC1 deregulation in the context of the full ClpC1P1P2 protease, we analyzed the degradation of model proteins upon incubation with dCym and Ecu*. For the model substrates α-casein and β-casein—which differ in their degree of compactness, secondary structure, and

(C and D) SEC elution profile of ClpC1 and ClpC1 F444A mutant. Size markers are indicated on top. Addition of dCym induces higher-order oligomers for ClpC1, whereas abolishing MD-MD contacts (F444A mutation) prevents oligomerization. All SEC runs were carried out in the presence of ATP, using the double Walker B (DWB) mutation that stabilizes the hexamer.

(E) Substrate degradation of two model substrates, β-casein and α-casein, by ClpC1P1P2 with or without dCym or Ecu*.

(F and G) Quantitative proteomics of *Msm* treated with 10 μM dCym/Ecu*. Data are normalized to the DMSO control. n = 3. See also Figure S1 and Table S1.

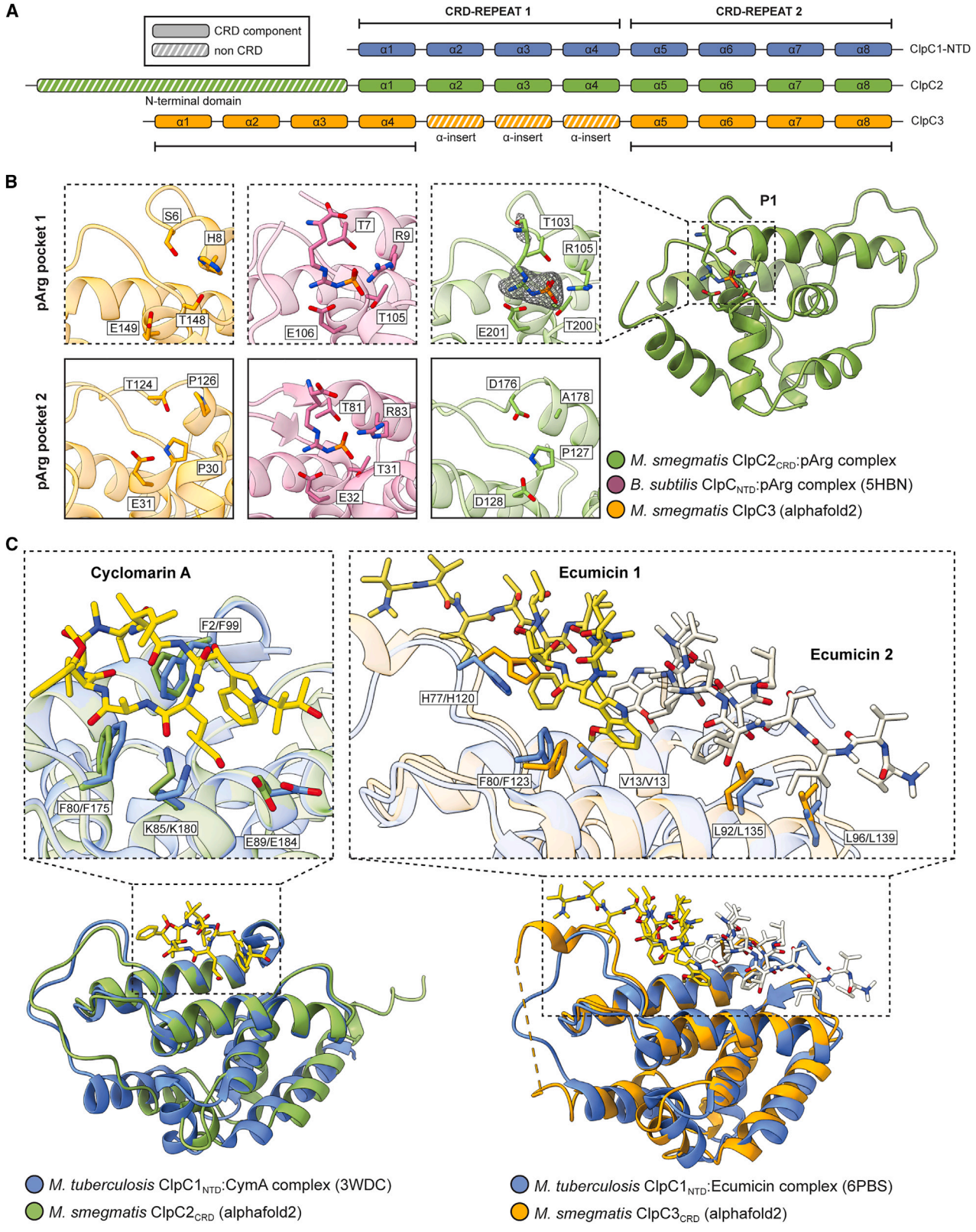

(legend on next page)

hydrophobicity—we observed notable differences. While dCym only accelerated degradation of α-casein, Ecu* exhibited dual effects. It inhibited the degradation of β-casein by ClpC1P1P2 but increased α-casein turnover (Figures 1E and S1F). These data immediately indicated a substrate-dependent mechanism of action for $ClpC1_{NTD}$-directed compounds. Given the disparate effects on the tested substrates *in vitro*, we performed quantitative MS to assess how Ecu* and dCym remodel the complete mycobacterial proteome. We incubated *Mycolicibacterium smegmatis* (*Msm*) cells with both compounds and performed label-free quantitative (LFQ) proteomics. Considering the cytotoxic effect of both antibiotics, we first screened for optimal conditions to characterize changes in proteome composition (Figures S1G and S1H). Under non-bactericidal conditions, neither Ecu* nor dCym treatment resulted in a significant deregulation of the mycobacterial proteome (Figures 1F and 1G). We did observe minor abundance changes, with several potential ClpC1P1P2 target proteins equally affected by Ecu* and dCym incubation (Table S1). However, we noted a remarkable exception to these subtle effects. Each antibiotic resulted in the selective and significant upregulation of one specific, unannotated target protein—one protein responding to each compound. Strikingly, the two proteins show clear homology to the $ClpC1_{NTD}$ domain, the receptor site targeted by the antibiotics. dCym treatment induced a strong increase of MSMEG_2792 (which we will refer to as ClpC2), while Ecu* incubation led to increased levels of MSMEG_3761 (which we will refer to as ClpC3).

In a second proteomics experiment, we used a longer incubation time and a higher, bactericidal dCym concentration. Prolonged incubation with dCym led to the depletion of a large fraction of mycobacterial proteins (Figure S1I). About 30% of the native proteome could no longer be identified by MS and was seemingly absent in bacteria treated for 6 h. Again, the most notable exception to the overall decrease in protein levels was ClpC2, which increased 600-fold in the presence of dCym. Indeed, ClpC2 was among the top 10 most abundant proteins in the dCym-treated mycobacterial cell, with absolute levels almost as high as those of ClpC1 (Figure S1J). In conclusion, our proteomics data show that dCym and Ecu* deregulate ClpC1P1P2, increasing overall protease activity and causing drastic proteome imbalances. Interestingly, this is accompanied by the selective and drastic enrichment of an uncharacterized pair of small Clp proteins, which both contain a $ClpC1_{NTD}$-like domain.

ClpC1, ClpC2, and ClpC3 share a common receptor domain

Phylogenetic analysis indicated that ClpC2 and ClpC3 are restricted to actinobacteria, whereas ClpC1 is much more widely distributed throughout actino- and Gram-positive bacteria. These data also show that ClpC1 and ClpC2 are present in the vast majority of actinobacteria, whereas ClpC3 is only present in a few genera without an obvious evolutionary pattern (Figures S2A and S2B). For example, *Msm* encodes a ClpC3 protein, but the closely related species *Mtb* does not. Sequence alignment of ClpC2, ClpC3, and $ClpC1_{NTD}$ revealed strong conservation of the annotated Clp repeat domain (CRD; sequence identify of 42% with ClpC2 and 39% with ClpC3, Figure S2A). This double 4-helix bundle is present as an N-terminal domain in most HSP100 chaperones, offering an extended surface for substrate binding.[31] ClpC2 contains an additional domain at its N-terminus, while ClpC3 instead has an extended insertion bridging the CRD-repeats between helices 4 and 5 (Figure 2A).

Sequence alignment also indicated that the receptor site for phospho-arginine (pArg), a ClpCP protease degradation signal,[10] is conserved in ClpC1 and ClpC2 but not in ClpC3 (Figure S2A). Though mycobacteria lack an ortholog of the protein arginine kinase McsB present in Gram-positive bacteria,[32,33] a recent proteomics study reported a multitude of pArg sites in *Msm* proteins.[34] These data suggest that the ClpC1P1P2 protease may utilize pArg as a degradation tag to recognize substrate proteins. Consistent with this idea, surface plasmon resonance (SPR) measurements showed that pArg binds strongly to $ClpC1_{NTD}$ and ClpC2 but not to ClpC3 (Table S2; Data S1A). To visualize the binding mode of pArg to ClpC2, we co-crystallized its CRD in complex with pArg and determined the crystal structure at 2.1 Å resolution (Figure 2B; Table S3). Superposition with the pArg complexes of *B. subtilis* ClpC (PDB 5hbn) confirmed the structural conservation of the receptor site, with all residues engaged in pArg binding found to be in a virtually identical position. The binding pocket, which exhibits characteristic electrostatic properties combining positively and negatively charged halves, is formed by the conserved residues Thr103, Arg105, Thr200, Glu201, which together accommodate the phospho-guanidinium group. Accordingly, ClpC2 could compete with ClpC1 for pArg-tagged client proteins. We thus hypothesize that the free substrate receptor modulates substrate binding to the mycobacterial ClpC1P1P2 protease.

To model the putative binding sites for dCym and Ecu*, we compared the structure of ClpC2 and the AlphaFold2 model of ClpC3 with co-crystal structures of ClpC1 ligand complexes (Figure 2C).[35] The dCym binding sites of ClpC2 and ClpC1 are almost identical, as are the binding sites for Ecu* in ClpC1 and ClpC3. Consistently, SPR binding studies revealed a strong binding of dCym to all three Clp proteins, with affinities in the low nM range. Ecu* also bound to the three proteins, albeit with slightly lower affinity (Table S2; Data S1A). Together, these data show that ClpC2 and ClpC3 share substrate-binding sites with ClpC1 and should thus have overlapping substrate selectivity. Modifications in these sites allow for specific differences in substrate selection as reflected by the interactions with the small-molecule ligands pArg, dCym and Ecu*.

Figure 2. CRD receptor domains of ClpC1, ClpC2, and ClpC3

(A) Structural organization of $ClpC1_{NTD}$, ClpC2, and ClpC3 highlighting the Clp repeat domain (CRD).

(B) Molecular model depicting the *Msm* $ClpC2_{CRD}$:pArg crystal structure. The two pArg binding pockets are shown next to it, together with the respective sites of $ClpC_{NTD}$:pArg and the modeled $ClpC3_{CRD}$.

(C) Superposition of *Mtb* $ClpC1_{NTD}$:CymA structure (PDB 3WDC) and $ClpC1_{NTD}$:ecumicin (PDB 6PBS) with ClpC2 and ClpC3, respectively. Conserved residues involved in antibiotic binding are indicated (first number, ClpC1). See also Figure S2, Tables S2 and S3, and Data S1A.

The CRD antibiotic-binding pocket is a receptor site for misfolded proteins

To explore the functional role of the CRD pocket targeted by cyclomarin A and ecumicin, we synthesized a linear ecumicin fragment (Ecu**) containing half of the ecumicin macrocycle, mimicking a natural peptide ligand. Upon confirming the binding of the short Ecu** peptide mimic (*N*-methylated LVAWG, Figure 3A) to $ClpC1_{NTD}$, (K_D = 50 μM, Table S2), we co-crystallized the protein: peptide complex and determined its crystal structure. Notably, peptide binding resulted in dimerization of $ClpC1_{NTD}$, with Ecu** wedged between the two antibiotic-binding sites (Figure 3B). Whereas side chains of *N*-Me-Leu1, *N*-Me-Ala3, and Gly5 were accommodated in the binding site of one protomer, residues Val2 and *N*-Me-Trp4 protruded into the partner $ClpC1_{NTD}$. Though we could not recapitulate binding with a canonical, non-N-methylated LVAWG peptide, the observed binding mode of the linear Ecu** peptide fragment pointed to a putative ClpC1P1P2 degron recognized by the CRD. Dimerization of $ClpC1_{NTD}$ modules could be instrumental in enlarging the binding pocket and achieving high affinity and specificity for cognate substrates. Consistent with our hypothesis, yeast Hsp104, containing a homologous N-terminal domain, utilizes a hydrophobic pocket equivalent to the antibiotic-binding site of ClpC1 to target client proteins[36] (Figure 3C). In fact, ClpC1 and ClpC2 contain functionally conserved Leu, Ile, and Val residues at the bottom of the same pocket, providing a potential interaction site for misfolded proteins. Superposition of the NTDs of ClpC1, ClpC2, and Hsp104 shows that dCym binding renders the hydrophobic pocket of ClpC1 and ClpC2 inaccessible to substrates (Figure S3A). To test the predicted Clp protein substrate recognition site *in vitro*, we performed competition experiments with ClpC1 antibiotics and model substrates (Figure S3B). In pull-down assays, we observed that ClpC2-CRD efficiently interacts with β-casein; however, addition of dCym markedly reduced the amount of bound substrate (Figure 3D). These data suggest that dCym and β-casein directly compete for the same binding site. In contrast, incubation of Ecu or dCym with the full-length ClpC1 unfoldase had mixed effects on the β-casein substrate (Figure 1E), likely due to the presence of receptor sites outside the CRD and the stimulatory effect of the two antibiotics on general ATPase activity (Figure S3C). Finally, we monitored β-casein degradation by ClpC1P1P2 over time, in the presence and absence of ClpC2-CRD (Figure 3E). These data revealed that ClpC2 interferes with ClpC1 substrate degradation, likely by competitive binding of the misfolded protein via the shared dCym binding site.

Taken together, our data suggest that ClpC1-directed antibiotics mimic the hydrophobic core of misfolded proteins that bind to the shared CRD in ClpC1, ClpC2 and ClpC3. To confirm this model, we performed a pull-down of tagged ClpC2 in a *Msm ΔclpC2* strain. As dCym binding was predicted to block interactions between ClpC2 and putative protein substrates, we compared the ClpC2 interactome of mycobacteria with and without dCym treatment (Figure S3D). Remarkably, treatment with dCym led to depletion of the most abundant interaction partners of ClpC2 (Figure 3F; Table S4). Among those interactors, nine proteins have been reported to be partially unfolded proteins preferentially targeted by ClpC1P1P2 and thus enriched in a ClpC1 depleted *Mtb* strain (Figure S3E).[37] We thus propose that ClpC2 competes with ClpC1 for the binding of unfolded proteins.

Together, our findings provide a mechanistic understanding of how dCym and other ClpC1-directed antibiotics interfere with the ClpC1P1P2 protease. The cyclic peptides function as small-molecule mimics of a misfolded protein, allowing them to hijack the bacterial PQC system. By binding to a conserved hydrophobic site in the CRD, used to bind aberrant proteins and activate unfoldase activity, the antibiotics exhibit a dual effect: they stimulate the Clp protease by inducing activated higher-order complexes and in parallel block access to misfolded proteins. Consequently, ClpC1-directed antibiotics cause drastic proteome imbalances leading to the downregulation but also upregulation of cellular targets.

ClpC2 functions as safeguard of the ClpC1P1P2 protease

To test the regulatory role of ClpC2 on the ClpC1P1P2 protease *in vitro*, we synthesized chemical adapters that contained either the pArg or dCym group as degron mimics. As a substrate anchor, we used JQ1, a chemical entity known to tightly bind to the bromodomain1 of BRDT ($BRDT_{BD1}$), our model substrate. Incubation of $BRDT_{BD1}$ with the bi-functional compounds thus yielded pArg and dCym-labeled protein (Figures 4A and S4A). Upon addition of a dCym-JQ1 degrader, we observed efficient degradation of the $BRDT_{BD1}$ substrate. However, substrate degradation by ClpC1P1P2 was strongly inhibited upon addition of equimolar amounts of ClpC2 (Figure 4A). Likewise, when we assayed $BRDT_{BD1}$ degradation in the presence of pArg-JQ1, we observed that ClpC2 was able to inhibit the Clp protease, buffering the introduced degradation tag (Figure 4B). These data suggest that ClpC2 functions as a competitive inhibitor for specific degrons recognized by ClpC1, sequestering potential substrates and preventing their degradation.

To investigate the biological consequences of ClpC2 and ClpC3 as competitive binders of ClpC1 in mycobacteria, we first tested the effect of the small Clp proteins on mycobacterial sensitivity to dCym and Ecu* antibiotics. We performed minimum inhibitory concentration (MIC) assays, using wild type (WT) and knockout *Msm* strains (*Δstrai*, *ΔclpC3*, and *ΔclpC2ΔclpC3*). In MIC assays, growth of the WT strain was inhibited at concentrations of 2.5 μM dCym or 6 μM Ecu*. Consistent with our *in vitro* data, genomic knockout of *clpC2* or *clpC3* each led to an increased sensitivity of mycobacterial cells against one of the antibiotics (Figures 4C and 4D). The *ΔclpC2* strain showed a 2-fold increase in sensitivity to dCym, while the *ΔclpC3* strain showed a 4-fold increased susceptibility to Ecu* treatment, with each antibiotic specificity corresponding to our earlier proteomics data (Figures 1F and 1G). Combined deletion of *clpC2* and *clpC3* did not further enhance sensitivity against either compound (Figures 4C and 4D). Moreover, we observed that overexpression of ClpC2 or ClpC3 strongly reduced dCym and Ecu* toxicity, respectively, allowing *Msm* growth at antibiotic concentrations 4-fold higher than those tolerated by WT cells. Elevating ClpC2 was more efficient in protecting cells from dCym, whereas ClpC3 upregulation led to higher resistance against Ecu*. Together our findings show that ClpC2 and ClpC3 can reduce the effective intracellular concentration of antibiotics that target the ClpC1 unfoldase. The small Clp proteins thus seem to

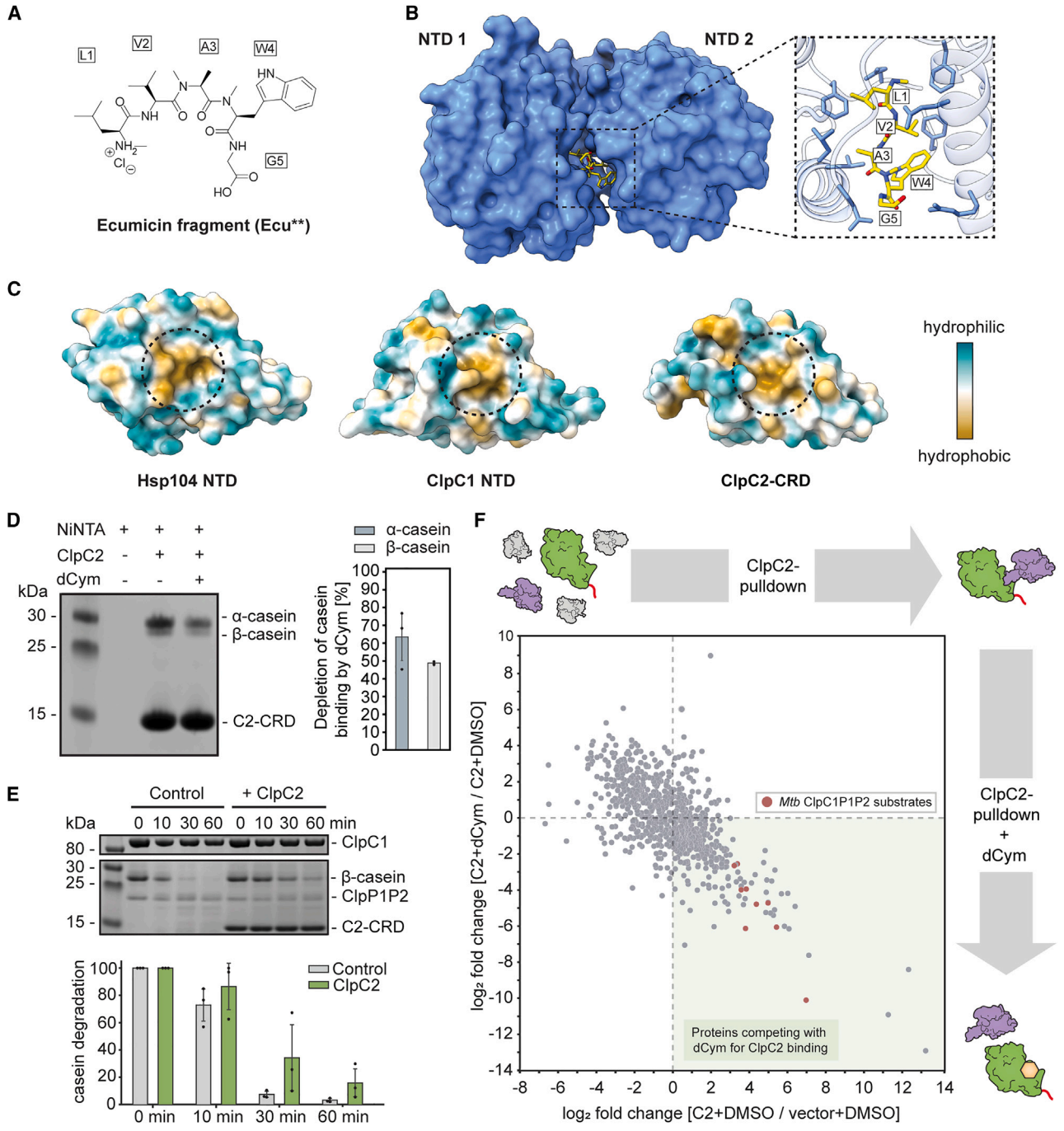

Figure 3. ClpC1-directed antibiotics bind to a hydrophobic pocket in ClpC1$_{NTD}$ used for substrate targeting

(A) Structure of the linear ecumicin fragment Ecu**.

(B) Co-crystal structure of the ClpC1$_{NTD}$:Ecu** complex. Ecu** is bound at the interface of two subunits, with its side chains protruding into the canonic antibiotic-binding sites.

(C) CRD comparison of ClpC1, ClpC2, and Hsp104 (PDB 5U2U), highlighting a common hydrophobic pocket.

(D) Pull-down assay using α- and β-casein as model substrates. Binding to ClpC2 is reduced upon dCym treatment (all proteins at 15 μM, dCym at 25 μM). Quantification represents mean ± SD, n = 3.

(E) *In vitro* degradation assay of β-casein by ClpC1P1P2 in presence of ClpC2. Quantification shows mean ± SD, n = 3.

(F) IP-MS analysis of ClpC2 pull-downs in *Msm*, in the absence (x axis) and presence of dCym (y axis). The most prominent interaction partners, enriched in the ClpC2 pull-down, were not bound to ClpC2 in the presence of dCym. These potential ClpC1 and ClpC2 substrates are seen in the lower right quadrant. Proteins identified in a previous *Mtb* ClpC1P1P2 substrate screen are highlighted in red. See also Figure S3 and Table S4.

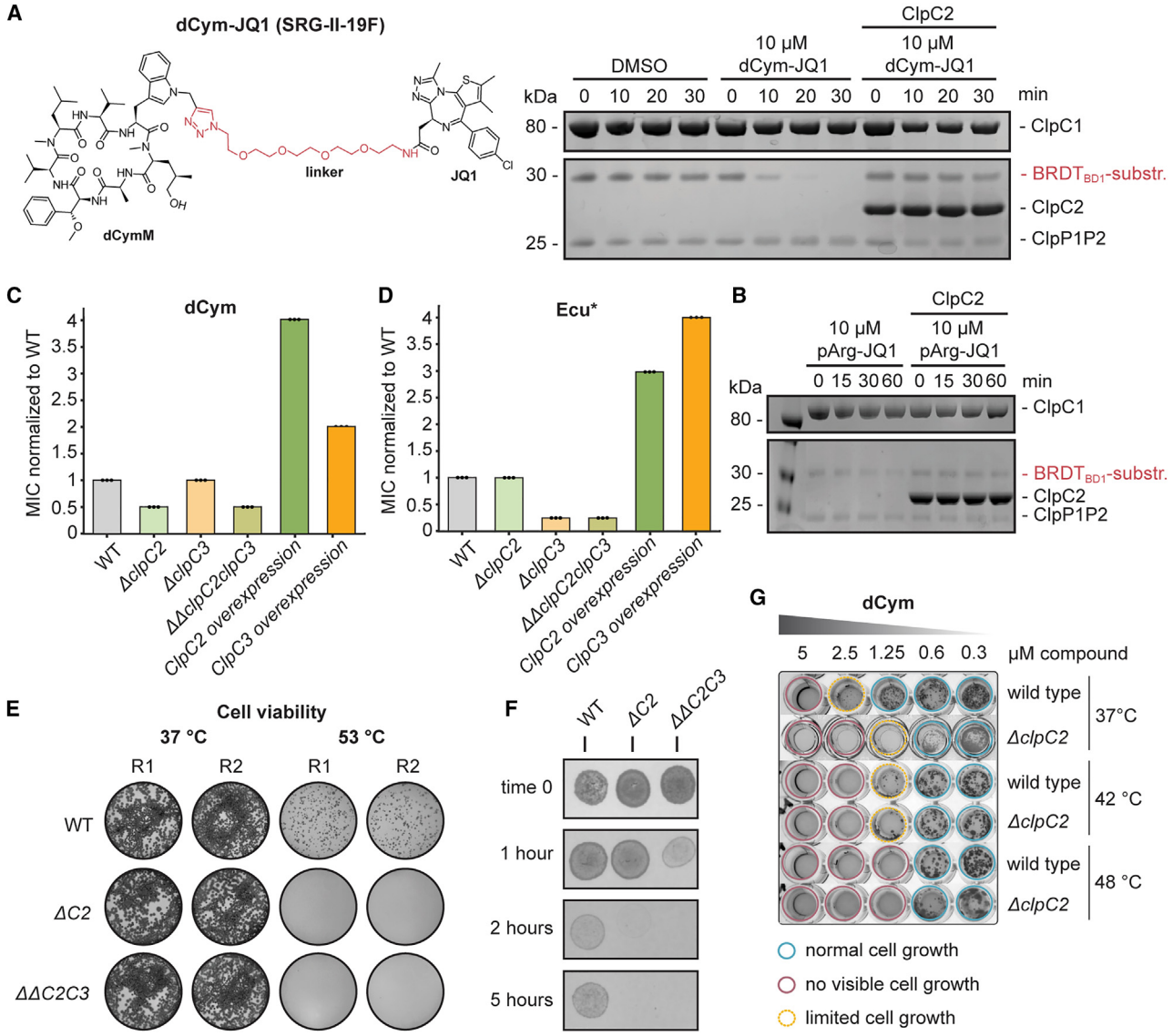

Figure 4. ClpC2 and ClpC3 protect ClpC1 from antibiotics and an overload with protein substrates in *Msm*

(A and B) (A) Degradation assay showing competition of ClpC2 and ClpC1 for the BRDT$_{BD1}$ model substrate labeled with the indicated dCym-JQ1 or (B) with pArg-dCym.

(C and D) MIC assay for dCym or Ecu* treated *Msm* WT and mutant strains. The MIC was visually determined, and bars indicate the first well in which inhibited cell growth was observed, normalized to WT. Uncropped plates are shown in Data S1B.

(E) Cell viability assay showing survival of *Msm* WT and mutants after heat shock (53°C for 4 h, replicates R1 and R2 from four independent biological replicates).

(F) MIT assay upon heat shock treatment. Survival was tested for *Msm* WT and mutants before (t0) as well as 1, 2, and 5 h after heat shock (53°C). n = 3.

(G) Checkerboard assay combining dCym treatment with heat shock conditions for *Msm* wild type and *ΔclpC2* mutant. 96-well plates were prepared with increasing temperature in the first dimension and reducing dCym concentrations in the second dimension (see also Data S1B for uncropped plates, n = 3). See also Figure S4.

represent specialized components of the PQC system that can be induced to counteract antibiotic activity in a specific manner. However, the molecular basis underlying their specific effects on dCym and Ecu* susceptibility in mycobacteria remained unclear. Given the ubiquitous distribution of ClpC2 in actinobacteria and the lack of ClpC3 in the major pathogen *Mtb H37Rv*, we therefore focused our subsequent analysis on the safeguarding role of the ClpC2 scavenger.

To further characterize the effect of ClpC2 on dCym, we performed an antibiotic kill curve assay, in which we followed the toxicity of dCym over time, as measured by colony-forming units (CFUs). While deletion of ClpC2 induced a cell growth inhibitory phenotype, treatment with dCym strongly exacerbated this effect. Upon incubation with dCym, viable *ΔclpC2* cells were reduced to ~30% control cells, as opposed to WT bacteria that were unaffected under these conditions (Figure S4B). These

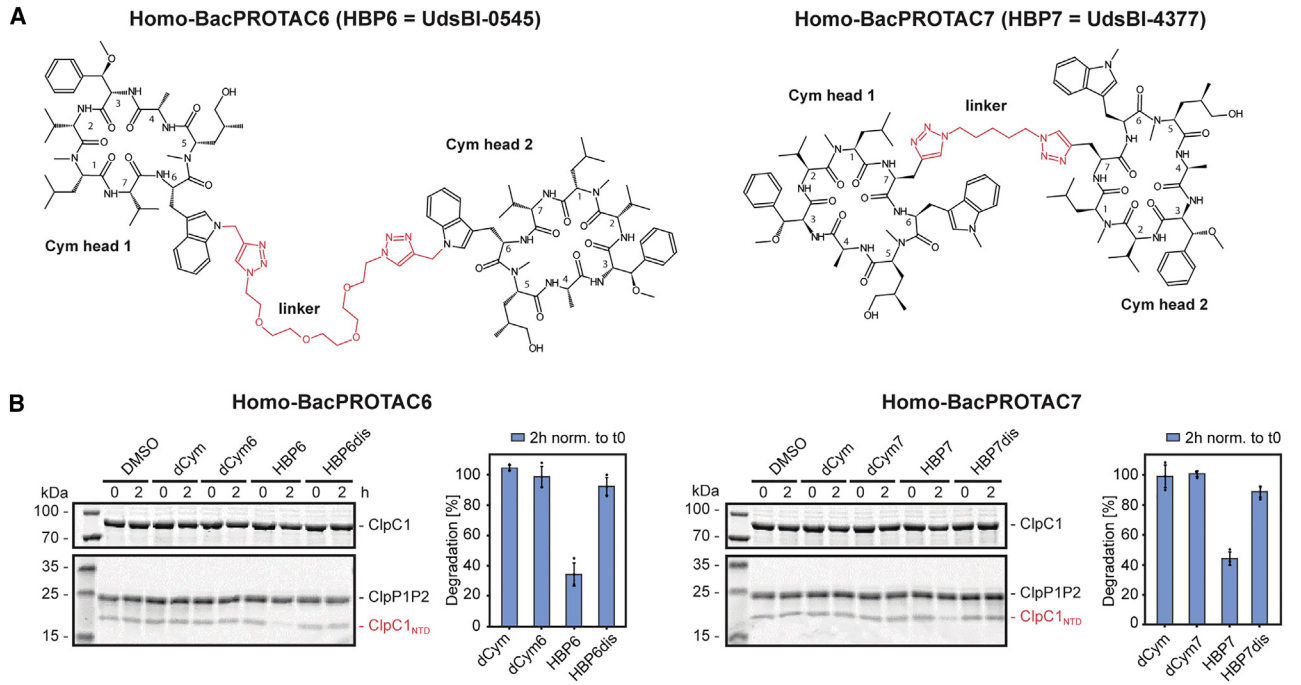

Figure 5. Induced degradation of the ClpC1$_{NTD}$ CRD by HBPs

(A) Chemical structure of HBP6 and HBP7, that differ in their linker attachment points and linker length. See Figure S6B for structures of dCym6 and dCym7.

(B) Degradation assay showing degradation of ClpC1$_{NTD}$, the CRD model substrate, by HBPs (100 μM). Quantification shows mean ± SD, n = 3. See also Figure S5.

data confirm that ClpC2 contributes to the mycobacterial defense against cyclomarin antibiotics. To test if ClpC2 exhibits a more general protective function within the mycobacterial PQC system, we performed kill curve assays for WT and mutants under heat shock conditions (53°C). Both *clpC2* and *clpC2/clpC3* knockouts showed complete lethality after a 4-h heat shock despite partial viability of the WT (Figure 4E). To verify the essentiality of ClpC2 for the stress response, we performed a minimum inhibitory time (MIT) assay monitoring the survival of bacteria over a 5-h heat shock time course. As expected, the *clpC2* mutants were impaired in growth as early as 1-h into heat shock, and both single and double mutants were substantially more sensitive to heat stress (Figure 4F). Finally, we analyzed the combined effect of heat stress and antibiotic treatment in a checkerboard assay. At 37°C, sensitivity to dCym was significantly higher in *clpC2* mutants than in WT. However, elevated temperatures also led to an increased antibiotic sensitivity in the WT strain (Figure 4G). Antibiotic sensitivity at 42°C was comparable to that of the *ΔclpC2* strain, implying that ClpC2 scavengers are fully occupied by heat-shocked proteins, leaving ClpC1 unprotected against dCym. Together, these data highlight the protective role of ClpC2 as a molecular chaperone, buffering stress-induced misfolded proteins as well as antibiotics mimicking the damaged substrates.

Dimeric Homo-BacPROTACs can target the Clp CRD motif *in vitro*

The protective function of ClpC2 relies on its ability to reduce the effective concentration of dCym and related compounds in the cell. In the presence of the scavenger protein, antibiotics must thus be applied in higher amounts to bind ClpC1 and deregulate its housekeeping function. We aimed to overcome the traditional occupancy-based mode of action of cyclomarin by developing event-driven antibiotics that inactivate ClpC1 in a catalytic manner. The recently developed BacPROTAC technology, which allows for the selective elimination rather than inhibition of target proteins, provided an attractive platform for this purpose. The technology relies on bi-functional chemical adapters that bind to a protein of interest (POI) and to the ClpC1$_{NTD}$ substrate receptor, thereby targeting POIs to the Clp protease and inducing their degradation. Importantly, the bi-functional adapters employ dCym derivatives (Figure S1A) that bind to the ClpC1$_{NTD}$. We thus hypothesized that a dimeric degrader containing two dCym heads, which we call HBP in analogy to Homo-PROTACs developed against the E3 component VHL,[38] could induce the degradation of ClpC1. In addition, the compound should be capable of targeting ClpC2 via its dCym binding site. Such dual action was hypothesized to be highly advantageous for the antibiotic activity potential of the HBP degrader, due to simultaneous elimination of the essential Clp protease and its security guard.

Guided by previously developed dCym degraders (Figure S1A),[26] we used either the tryptophan derivative at position 6 or the valine at position 7 as linker attachment points to generate the dimeric HBP6 and HBP7, respectively (Figure 5A; chemical synthesis described in Junk et al.[29]). As a control for selective targeting of the Clp CRD, we fused two distomeric variants of the cyclic peptides, in which all stereocenters are inverted

(Figures S5A and S5C). SPR measurements confirmed that the functional HBP variants bind to $ClpC1_{NTD}$ and ClpC2 with high affinity ($K_D \sim 0.5–2.5$ nM), whereas their distomeric counterparts did not interact with the Clp proteins (Table S2; Data S1A). To estimate the activity of HBPs *in vitro*, we followed ClpC1P1P2 mediated degradation of $ClpC1_{NTD}$. Incubation with HBPs induced elimination of about 80% of the $ClpC1_{NTD}$ substrate (Figure 5B). In contrast, the distomeric controls could not redirect the ClpC1P1P2 protease, excluding indirect effects on substrate depletion. These *in vitro* degradation experiments indicate that HBPs can mark CRD-containing proteins for degradation.

Homo-BacPROTACs reduce the levels of ClpC1 and ClpC2 in *M. smegmatis*

To study whether HBPs could target CRD-containing Clp proteins in mycobacteria, we used *Msm* as a model system. Active HBP compounds had a similar MIC as the parent monomers, indicating that despite their large size, the applied compounds are taken up by mycobacteria (Figures S5B and S6A; for detailed characterization of HBP structure-activity relationships see Junk et al.[29]). To study their *in situ* activity, we carried out an LFQ MS experiment, monitoring changes in the *Msm* proteome upon HBP treatment. As control, we used the inactive HBP distomers, which did not exhibit a bacteriotoxic effect, as well as dCym monomers bearing alkyne groups at the points of linker attachment. Overall, the MS data indicated that monomeric and dimeric dCym variants led to gross perturbation in the proteome. Treatment with both the HBPs and their monomeric heads led to a strong increase of ClpC2 levels, while addition of distomeric controls did not raise ClpC2 abundance (Figures 6A, 6B, and S6B). Importantly, however, only in the case of active HBP dimers did we observe a significant decrease in ClpC1 levels. Moreover, when we compared the ClpC2 levels upon treatment with monomeric dCym and dimeric HBP, we observed that the relative levels of ClpC2 are markedly reduced in the presence of the degrader, evidencing simultaneous targeting of ClpC1 and ClpC2 (Figure 6A). To confirm the proteomics data, we employed a parallel reaction monitoring (PRM) protocol to follow ClpC1 and ClpC2 over time. The quantitative MS data confirmed that both ClpC1 and ClpC2 levels are diminished upon incubation with the dimeric BacPROTACs as compared with the monomeric compounds (Figure 6B). After 24 h, levels of ClpC1 were reduced to ~40%, whereas ClpC2 levels decreased by 45%–60%, as compared with cells treated with monomeric dCym. Together these data highlight the potential of HBP degraders to target the essential ClpC1 unfoldase together with the ClpC2 security guard. However, in *Msm*, this activity seems to be masked by the strong upregulation of ClpC2 upon antibiotic treatment, sequestering the degrader. To confirm its protective role, we studied the effect of HBPs in the *ΔclpC2 Msm* knockout strain. As reflected by MIC_{50} values, the active synthetic degraders had a 7-fold higher potency in the *ΔclpC2* strain than in the WT (Figures 6C and S6C). Compared with the milder effect for the monomeric antibiotic (only 2-fold higher sensitivity in *ΔclpC2*, Figure 4C), these data point to a distinct mode of action of the HBP degrader and highlight its improved efficacy in targeting ClpC1. To further confirm the role of ClpC2 in buffering misfolded proteins and protecting against antibiotics targeting ClpC1, we followed the potency of HBPs under heat shock conditions. Stress-induced protein damage should enhance the load on the PQC system and limit the ability of ClpC2 to protect ClpC1. Consistently, we see that the efficacy of HBPs is drastically improved during heat shock, more than that of the isolated dCym compound (Figure 6D). This disparity further highlights the distinct mode of action of the monomeric and dimeric antibiotics: the bivalent HBP exhibits a dual activity, deregulating and degrading the PQC components ClpC1 and ClpC2.

Homo-BacPROTACs are potent antibiotics killing pathogenic *M. tuberculosis*

Having shown the BacPROTAC induced degradation of ClpC1 and ClpC2 in *Msm*, we tested their potency against the virulent *Mtb* strain H37Rv, a model strain used to explore the effect of antitubercular compounds on pathogenicity. *Mtb* encodes a ClpC2 ortholog that is closely related to the *Msm* ClpC2 (62% sequence identity, 82% homology) but no ClpC3 and expresses a ClpC1 unfoldase containing an N-terminal CRD identical to its *Msm* counterpart. To profile cellular targets of cyclomarin A, we performed pull-down assays with *Mtb* lysates using a biotin probe connected to a simplified cyclomarin derivative.[26] Upon elution with the cyclic peptide, we identified ClpC1 and ClpC2 as main interactors of the cyclomarin derivative (Figure S7A). As expected, *Mtb* ClpC2 also uses its conserved receptor site to bind ClpC1-directed antibiotics. To investigate the antitubercular activity of HBP degraders, we performed dose response curves in *Mtb* WT and *ΔclpC2* deletion strains. Dimeric HBP6 and HBP7 strikingly outperformed the monomer (dCymM) in terms of antibiotic activity, with 115- and 150-fold higher potency, respectively (Figures 7A and S7B). Indeed, the antibacterial effect of dCym monomers was comparable between *Mtb* and *Msm* (MIC_{50} about 10–40 μM), while the pathogenic *Mtb* was much more sensitive to HBP degraders, with low MIC_{50} values ranging from 0.26 to 0.34 μM.

To demonstrate that the antibiotic effect of HBPs is due to ClpC1 degradation, we performed quantitative proteomics comparing active and inactive BacPROTACs. In line with the pronounced toxicity of HBPs toward *Mtb*, we observed a higher ClpC1 degradation efficiency of HBPs in *Mtb* compared with *Msm*, with a 5-fold reduction in ClpC1 levels (Figures 7B and 7C). To estimate the effect of the degrader on ClpC2 levels, we employed a *ΔclpC2* strain, in which the bulk of the Clp protein is absent and thus not responsive to antibiotic-mediated degradation, while a short N-terminal remnant (21 residues; $ClpC2_{NT}$) is still expressed from the endogenous promotor. Proteomics analysis revealed that HBP treatment triggered a 20-fold increase in $ClpC2_{NT}$ levels in the *Mtb ΔclpC2* mutant, presumably resulting from transcriptional upregulation, similar to what we observed in *Msm*. In contrast, treatment of WT cells with HBPs led to a much smaller increase in ClpC2 levels. Compared with $ClpC2_{NT}$ (*ΔclpC2* strain), the amounts of ClpC2 were 5-fold less elevated in WT, suggesting that the dimeric BacPROTAC can target ClpC2 via its CRD and induce its degradation in *Mtb* (Figures 7C, S7C, and S7D). Thus, our data demonstrate that HBPs are potent antitubercular compounds, exhibiting a 115-fold higher potency than parent cyclomarin A compounds. The strongly increased efficacy relies on their distinct mode of

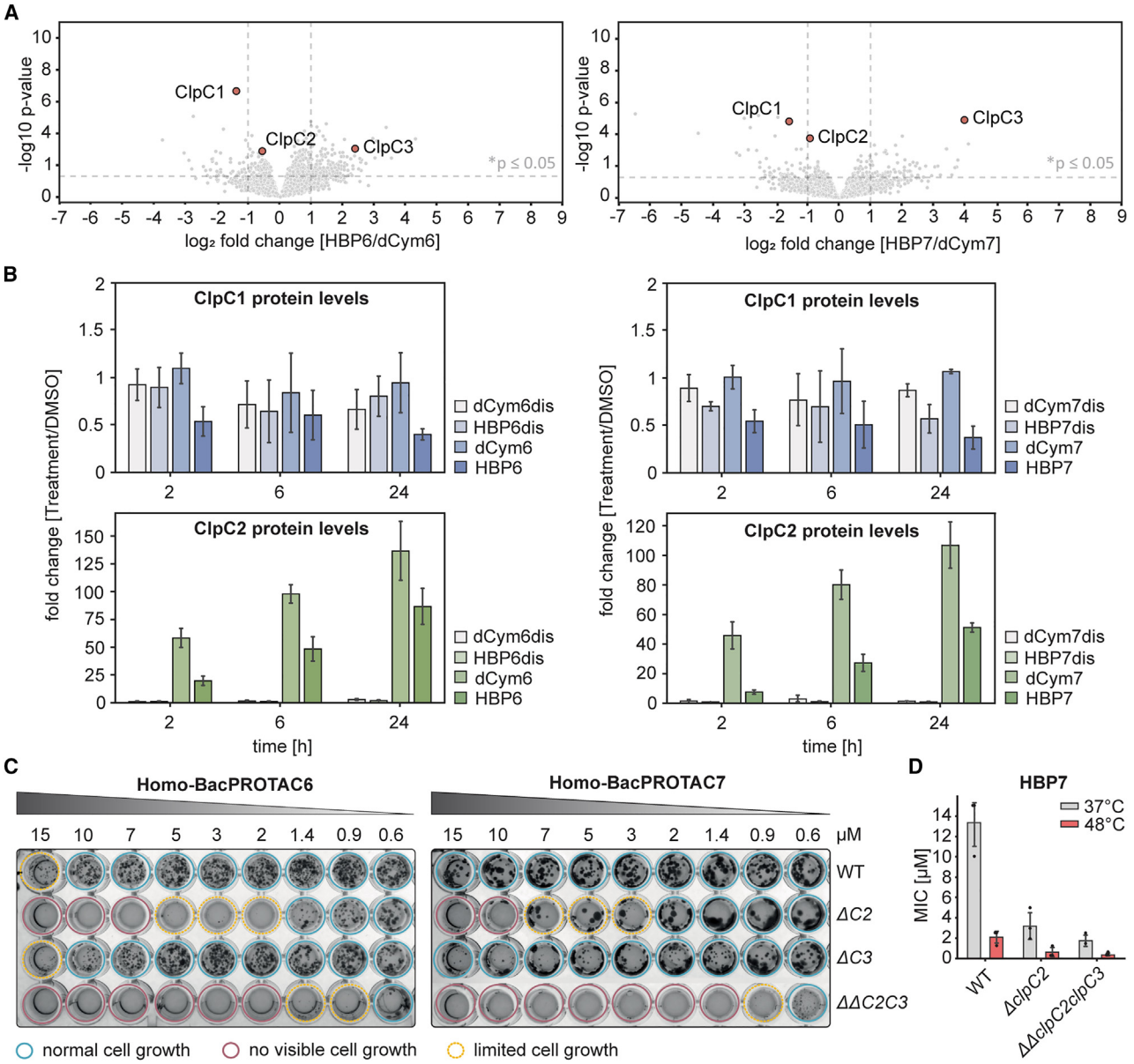

Figure 6. Degradation of ClpC1 and ClpC2 by HBPs in *Msm*

(A) Quantitative proteomics of *Msm* cells treated with HBP6 and HBP7 (12.5 μM, 24 h) normalized to incubation with their monomeric head groups (dCym6 and dCym7). ClpC1 levels decreased to 38% and 34%, whereas ClpC2 levels decreased to 68% and 51%, respectively, upon HBP treatment, in comparison with monomer treatment. n = 3.

(B) PRM analysis of Msm treated with 12.5-μM HBP6 or HBP7. ClpC1 and ClpC2 levels were analyzed over time, confirming ClpC1 and ClpC2 reduction upon incubation with HBP degraders, compared with monomeric and inactive controls. Results are mean ± SD, n = 3.

(C) MIC assays for HBP6 and HBP7, comparing *Msm* mutants with WT. n ≥ 5.

(D) Checkerboard assay combining HBP treatment with heat shock conditions for *Msm* WT and mutants. Plates were prepared with reducing HBP concentrations and placed overnight at 48°C. Afterward, the plates were transferred to 37°C until colonies appeared. Displayed are the mean ± SD, n = 3. See also Data S1B for uncropped plates, and Figure S6.

action, inducing degradation of the housekeeping proteins ClpC1 and ClpC2 rather than inhibiting them.

Given the importance of antibiotic resistance to *Mtb* pathogenesis, we next aimed to assess resistance development against these BacPROTAC degraders. We treated *Mtb* H37Rv with either HBP6 or HBP7 on solid media (at concentrations of ≥ 6 × MIC). In total, we obtained four spontaneous resistant clones, all showing reproducible growth in presence of the two BacPROTACs and exhibiting cross-resistance against HBP6 and HBP7 (Figures 7D and S7E). Whole-genome sequencing revealed that the three HBP6 mutant clones had the same mutation in *clpC1*, resulting in an F80V substitution in the $ClpC1_{NTD}$

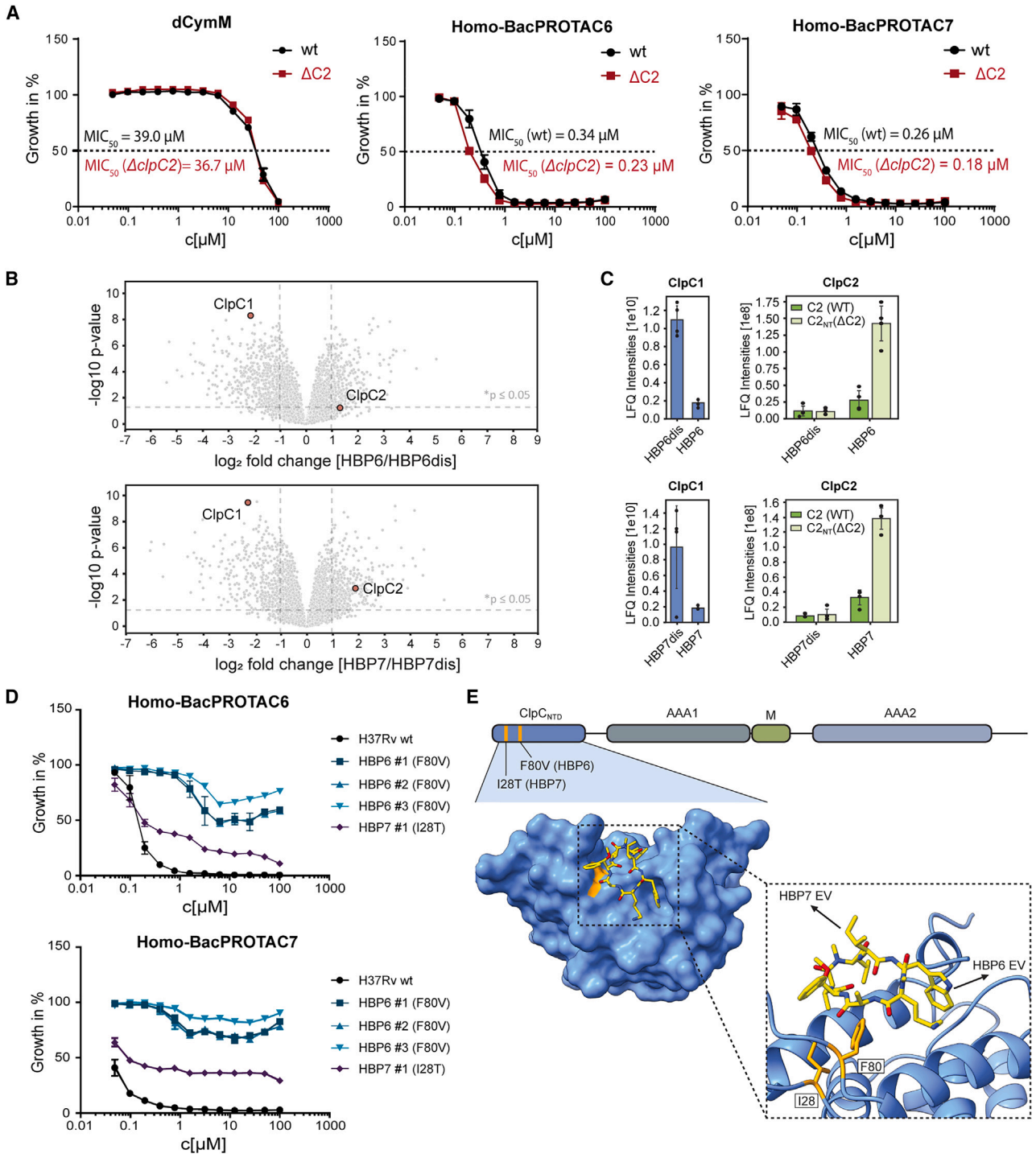

Figure 7. Homo-BacPROTAC treatment impairs growth of *M. tuberculosis*

(A) Dose response curves comparing dCymM monomer and HBP degraders on *Mtb* growth and comparing WT *Mtb* with the *ΔclpC2* mutant. Cells show a 115-fold (WT) and 160-fold (*ΔclpC2*) higher sensitivity to HBP6 compared with dCymM. The mutant is slightly more sensitive than the WT, consistent with the lack of ClpC2's protective function. Results are mean ± SD, n = 3.

(B) Quantitative proteomics of *Mtb* cells treated with HBP6 and HBP7, normalized to treatment with inactive distomers (HBP6-dis, HBP7-dis). Quantification shows mean ± SD, n = 3.

(C) LFQ intensities comparing ClpC1 (left) and ClpC2 (right) degradation induced by HBPs and their corresponding distomers. For quantitative proteomics of *Mtb* WT and *ΔclpC2* cells, the latter was expressing a truncated 21-aa ClpC2 peptide ($ClpC2_{NT}$). While ClpC1 is reduced to similar levels in treated WT and *ΔclpC2*

(legend continued on next page)

(Figure 7E). Phe80 is located at the bottom of the hydrophobic pocket targeted by the cyclic peptide antibiotics, and the critical role of Phe80 in binding cyclomarin A has been previously shown in targeted *in vitro* and *in vivo* interaction studies, where the F80A mutation abolished antibiotic binding.[24] Accordingly, the F80V mutation is expected to markedly reduce HBP affinity for ClpC1, explaining the evolved antibiotic tolerance. The sequenced HBP7 clone, which exhibited weaker resistance against the two HBPs, revealed another mutation, I28T, in the $ClpC1_{NTD}$ (Figures 7D and 7E). The mutated Ile28 is located in close proximity to Phe80, such that the introduced threonine may induce slight rearrangements in the cyclomarin binding pocket corresponding to moderate resistance.

Non-replicating bacteria pose a further challenge to the activity of BacPROTACs, as these persisters are well-known for escaping antibiotic treatment. To investigate HBP potency in dormant cells, we tested pathogenic *Mtb* in a checkerboard assay, in which HBPs were combined pairwise with bedaquiline. By inhibiting the ATP synthase subunit C (AtpE), bedaquiline induces lower intracellular ATP levels, resembling a dormant state in *Mtb*.[40–42] However, treatment of *Mtb* H37Rv cells with bedaquiline had no effect on HBP7 BacPROTAC activity, demonstrating that HBPs work equally well—or even better—as the reference drug rifampicin against persistent cells (Figure S7F).

Together these data reveal ClpC1 as an attractive antibiotic target and confirm the role of the $ClpC1_{NTD}$ in binding BacPROTACs. Considering the threat of persistent bacteria in clinics, our findings further suggest BacPROTACs as promising therapeutic agents that could retain activity against dormant *Mtb* latent in host cells.

DISCUSSION

Perhaps the most threatening bacterial pathogen with regard to antibiotic resistance and infection severity is *Mtb*, the cause of TB. In addition to the long and complex treatment routines required for established antibiotics, second-line TB drugs, including cycloserine, capreomycin, and quinolones exhibit serious side effects that limit their utility. Therefore, novel antitubercular compounds with distinct modes of action able to evade drug resistance are urgently needed.[43] In this study, we pioneered a BacPROTAC antibiotic that overcomes a bacterial PQC security system, is also active in bacteria with a dormant-like phenotype and targets multiple components of the mycobacterial stress response concurrently.

As a critical first step, we revealed the mode of action of ClpC1-directed antibiotics. Our data delineate the dual mechanism employed by cyclomarin A and related antibiotics (ecumicin, rufomycin, and lassomycin), all of which bind to a conserved site at the $ClpC1_{NTD}$ substrate receptor. We show that peptide antibiotics mimic exposed hydrophobic residues of unfolded proteins and bind to a common pocket in HSP100 chaperones. Using substrate mimicry, the antibiotics can hijack the ClpC1P1P2 protease, which performs an essential housekeeping role in mycobacteria.[37] The antibiotics act as competitive inhibitors for misfolded proteins and in parallel, remodel ClpC1 into its active higher-order oligomer state, yielding a permanently activated protease that degrades cellular proteins in an unselective manner. Due to this bimodal activity, dCym treatment leads to massive perturbations in the proteome, as reflected by the up- and downregulation of key cellular factors. Importantly, proteomic analysis identified two small Clp proteins, ClpC2 and ClpC3, that were specifically upregulated upon either cyclomarin A or ecumicin treatment. Characterization of these factors uncovered a bacterial security system that protects the essential ClpC1P1P2 protease. We show that the well-conserved ClpC2 is a specialized Clp regulator. It functions as a scavenger protein shielding the ClpC1P1P2 protease from a surplus of binding partners by using equivalent receptor sites. Deletion of ClpC2 induces a severe thermosensitive phenotype and is lethal under extreme heat shock, suggesting that ClpC2 sequesters misfolded proteins and prevents an overload of the housekeeping protease during proteotoxic stress. Moreover, ClpC2 can sequester antibiotics like CymA that act as small-molecule mimics of a misfolded protein. Binding to ClpC2 lowers the intracellular concentration of the antibiotic and thus ameliorates its impact on ClpC1 and the protease. Due to its protective function, ClpC2 must be considered when developing antibiotics targeting the mycobacterial stress response machinery.

To efficiently shut down the PQC system, we developed bivalent HBP degraders targeting the common Clp receptor domain, CRD. In pathogenic *Mtb*, this pan-degrader exhibited strong antibacterial potency, inhibiting bacterial growth >100-fold more efficiently than the natural monomeric cyclic peptide. By fusing two dCym heads, the bivalent compound redirects the ClpC1P1P2 protease against itself, inducing degradation of ClpC1. Thus, antibiotic activity relies on the auto-knockdown of an essential proteolytic machine. Moreover, HBP degraders reduced not only the level of ClpC1 but also that of its safeguarding protein ClpC2. The simultaneous targeting of the Clp protease and its security system underlies the extraordinary power of the HBP as an antibiotic. We hypothesize that the more pronounced antibiotic effect of HBPs toward *Mtb* compared with *Msm* is due to different cellular levels of ClpC2, leading to more efficient degradation of the ClpC1 unfoldase and a concomitant reduction of the MIC from ~15 μM in *Msm*

bacteria, levels of ClpC2 (WT) and $ClpC2_{NT}$ (*ΔclpC2*) are strikingly different. This difference likely reflects induced degradation of ClpC2 in WT cells, whereas the $ClpC2_{NT}$ peptide is inaccessible to HBP-mediated degradation. Quantification shows mean ± SD, n = 3.

(D) Dose response curves comparing compound susceptibility of four *Mtb* spontaneous resistant mutants against HBPs, carrying different single nucleotide polymorphisms (SNPs, T>G at nucleotide 238 causing F80V: HBP6 #1-#3; T>C at nucleotide 83 causing I28T: HBP7 #1). Mutation of F80 leads to strong growth rescue against treatment with either of the BacPROTACs, which is less pronounced for the I18T mutant. Results are mean ± SD, n = 3. Notably, the sequencing also revealed a second-site deletion in the mycocerosic acid synthase (*mas*) gene, which is involved in biosynthesis of the cell wall lipid phthiocerol dimycocerosate (PDIM), causing a frameshift in all three HBP6 resistant clones. However, since mutations causing PDIM loss are known to occur frequently during *in vitro* culturing of *Mtb* strains,[39] since the mutants show unaltered susceptibility profiles toward other antibiotics, and since the HBP7 resistant clone harbored no mutations in the PDIM biosynthetic gene cluster, the *mas* mutation likely had no effect on the resistance mechanism (Figure S7E).

(E) Resistance mutations against HBP6 (F80V) and HBP7 (I28T) mapped to the crystal structure of $ClpC1_{NTD}$:CymA analog (PDB 7AA4). Mutated residues are highlighted in orange. Arrows indicate the exit vector (EV) positions of HBP6 and HBP7. See also Figure S7.

to ~0.2 μM in *Mtb*. It should also be noted that, in addition to its degrader function, the potency of HBP is enhanced by the inherent cytotoxicity of the incorporated cyclomarin derivatives, which interfere with ClpC1-mediated protein degradation. Thus, the degrader benefits from a dual activity, simultaneously deregulating and destroying a central component of the mycobacterial PQC system. In related medicinal chemistry studies,[29] we found that even intracellular *Mtb* propagating in infected THP-1 cells showed a concentration-dependent reduction in CFU after incubation with HBPs. Moreover, the degrader molecules exhibited promising pharmacokinetic properties and minimal cytotoxicity in a macrophage infection model, as compounds were well-tolerated at the highest concentration tested (50 μM[29]). We conclude that the BacPROTAC approach presents an effective strategy to develop anti-mycobacterial agents, enabling the degradation of essential Clp proteins. Considering the >100-fold increased efficacy of bivalent HBPs over the parent CymA compound, the mechanistic advantages of small-molecule degraders over classic drugs seems to be conserved in BacPROTACs, providing an attractive technology platform to develop next generation antibiotics.

Limitations of the study

Although our study identifies ClpC2 and ClpC3 as specific scavenger proteins against the antitubercular compounds cyclomarin A (dCym) and ecumicin (Ecu*), respectively, their exact molecular mechanism was not fully resolved. For example, the molecular mechanism leading to upregulation of ClpC2 and ClpC3 by dCym and Ecu* has remained elusive. While our data point to transcriptional regulation, the exact nature of these regulatory factors, the identity of the respective stress operon, and their interaction with the small Clp proteins requires further study. Moreover, our *in vitro* studies show that dCym and Ecu* have similar affinities for ClpC2 and ClpC3. Therefore, it is unclear why treatment with these antibiotics leads to the selective upregulation of one of two distinct proteins, which seem to counteract antibiotic activity in a specific manner in the mycobacterial cell. Though our study highlights the underestimated complexity of the mycobacterial stress response system, better understanding of this system and the involved factors will be critical to unleash the full potential of ClpC1-directed antibiotics and small-molecule degraders.

With regard to the degrader mechanism, it should be noted that the binding of HBPs to adjacent CRDs, like those present in the ClpC1 hexamer or ClpC2 dimer, may limit their availability for targeting ClpC1 and ClpC2 subunits in *trans* and directing them for degradation. The intra-molecular ClpC1-ClpC1 and ClpC2-ClpC2 associations may explain the discrepancy between HBP-binding affinity *in vitro* and lower efficacy in cells. Although we consider linker design as a promising strategy to prevent intra-molecular HBP recruitment and enhance degradation activity, addressing this point experimentally is challenging due to the dynamic nature of ClpC1 and ClpC2 oligomers.

STAR★METHODS

Detailed methods are provided in the online version of this paper and include the following:

- KEY RESOURCES TABLE
- RESOURCE AVAILABILITY
  - Lead contact
  - Materials availability
  - Data and code availability
- EXPERIMENTAL MODEL AND SUBJECT DETAILS
- METHOD DETAILS
  - Isolation of chromosomal DNA
  - Construction of mycobacterial mutants
  - Cloning of overexpression constructs
  - Protein expression and purification
  - Surface plasmon resonance (SPR)
  - Analytical size exclusion chromatography (aSEC)
  - Negative staining EM
  - *In vitro* substrate degradation assay
  - *In vitro* ClpC2 pulldown
  - Co-crystallization and structure determination
  - *M. smegmatis* sample preparation for MS analysis
  - Whole cell proteomics & PRM sample preparation
  - Immunoprecipitation (IP) sample preparation
  - Sample quality control for MS analysis
  - Label free quantification mass spectrometry
  - LFQ-MS and IP-MS data analysis
  - Parallel reaction monitoring (PRM) analysis
  - PRM data analysis
  - *M. tuberculosis* samples for MS analysis
  - Pull-down assays in *M. tuberculosis*
  - Whole cell MS from *M. tuberculosis*
  - Minimum inhibitory concentration (MIC) assay
  - Dose response curves in *M. tuberculosis*
  - Checkerboard assay
  - Kill curve assay
  - Minimum inhibitory time (MIT) assays
  - Resistance screens and WGS in *M. tuberculosis*
  - Chemical Synthesis of Ecu**
  - Chemical Synthesis of dCym-JQ1 (SRG-II-19F)
  - 2-((*S*)-4-(4-Chlorophenyl)-2,3,9-trimethyl-6*H*-thieno[3,2-f][1,2,4]triazolo[4,3-a][1,4]diazepin-6-yl)-N-(14-(4-((3-(((2S,5*S*,8*S*,11*S*,14*S*,17*S*,20*S*)-5-((*R*)-3-hydroxy-2-methylpropyl)-17-isobutyl-14,20-diisopropyl-11-((*R*)-methoxy(phenyl)methyl)-4,8,16-trimethyl-3,6,9,12,15,18,21-heptaoxo-1,4,7,10,13,16,19-heptaazacyclohenicosan-2-yl)methyl)-1*H*-indol-1-yl)methyl)-1*H*-1,2,3-triazol-1-yl)-3,6,9,12-tetraoxatetradecyl)acetamide (dCym-JQ1 / SRG-II-19F)
  - Synthesis of pArg-JQ1 (BI01826025)
- QUANTIFICATION AND STATISTICAL ANALYSIS

SUPPLEMENTAL INFORMATION

Supplemental information can be found online at https://doi.org/10.1016/j.cell.2023.04.009.

ACKNOWLEDGMENTS

We thank all members of the Clausen group for remarks on the manuscript and Alexander Schleiffer for help with sequence analyses. We thank Juliane Kley for help with crystallization. We acknowledge DESY (Hamburg, Germany) for the provision of experimental facilities at beamline P11 and we would like to thank Johanna Hakanpää for assistance. We thank Stacie Dodgson from

Life Science Editors for editorial assistance. M.K. and D.P. acknowledge funding from the Deutsche Forschungsgemeinschaft (CRC1430), R.K. from the Deutsche Forschungsgemeinschaft (grant number KA 2259/5-1) and the Jürgen Manchot Stiftung (graduate school MOI IV), and M.K. acknowledges funding by INST FUGG for purchasing Lumos MS. This work was further supported by the European Research Council (AdG 694978, T.C.), an FFG Headquarter Grant (no 852936, to T.C.), the Vienna Science and Technology Fund (WWTF 10.47379/LS21029, to T.C., M.H., and M.K), Boehringer Ingelheim (to J.L. and S.J.), and the National Health and Medical Research Council (Investigator grant APP1174941 to R.J.P). F.E.M., J.L., and S.J. are members of the Boehringer Ingelheim Discovery Research global post-doc program. The IMP is supported by Boehringer Ingelheim.

AUTHOR CONTRIBUTIONS

D.M.H., S.J., L.J., A.M., R.K., R.J.P., G.B., U.K., and T.C. designed experiments; L.J., P.M.E.H., S.K., M.K., S.G., and V.M.S. performed the chemical synthesis of the cyclomarin A, ecumicin, and BacPROTAC variants; D.M.H., K.F., J.L., F.E.M., and K.R. performed biochemical assays and binding measurements; K.F. and K.R. contributed to biophysical profiling of BacPROTACs; D.M.H. performed the EM analysis, A.M. the crystallographic analysis; S.J., J.L., K.F., K.S., and L.v.G. prepared bacterial strains and carried out the analyses in bacteria; D.M.H., S.J., D.P., F.K., and M.H. performed the mass spectrometry analysis; T.C., G.B., U.K., and H.W. co-coordinated the research collaborations between Boehringer Ingelheim, IMP, and Saarland University; T.C. coordinated the research project and prepared the manuscript together with D.M.H. and S.J., with input from all authors.

DECLARATION OF INTERESTS

K.F., V.M.S., K.R., H.W., and G.B. were employees of Boehringer Ingelheim at the time of this work.

Received: October 11, 2022
Revised: February 24, 2023
Accepted: April 5, 2023
Published: May 2, 2023

REFERENCES

1. Hutchings, M.I., Truman, A.W., and Wilkinson, B. (2019). Antibiotics: past, present and future. Curr. Opin. Microbiol. *51*, 72–80. https://doi.org/10.1016/j.mib.2019.10.008.
2. Lewis, K. (2020). The science of antibiotic discovery. Cell *181*, 29–45. https://doi.org/10.1016/j.cell.2020.02.056.
3. Allué-Guardia, A., García, J.I., and Torrelles, J.B. (2021). Evolution of drug-resistant Mycobacterium tuberculosis Strains and Their adaptation to the human lung environment. Front. Microbiol. *12*, 612675. https://doi.org/10.3389/fmicb.2021.612675.
4. Cheesman, M.J., Ilanko, A., Blonk, B., and Cock, I.E. (2017). Developing new antimicrobial therapies: are synergistic combinations of plant extracts/compounds with conventional antibiotics the solution? Pharmacogn. Rev. *11*, 57–72. https://doi.org/10.4103/phrev.phrev_21_17.
5. Igarashi, M., Ishizaki, Y., and Takahashi, Y. (2017). New antituberculous drugs derived from natural products: current perspectives and issues in antituberculous drug development. J. Antibiot. (Tokyo) *71*, 15–25. https://doi.org/10.1038/ja.2017.126.
6. Miethke, M., Pieroni, M., Weber, T., Brönstrup, M., Hammann, P., Halby, L., Arimondo, P.B., Glaser, P., Aigle, B., Bode, H.B., et al. (2021). Towards the sustainable discovery and development of new antibiotics. Nat. Rev. Chem. *5*, 726–749. https://doi.org/10.1038/s41570-021-00313-1.
7. Song, W.M., Zhao, J.Y., Zhang, Q.Y., Liu, S.Q., Zhu, X.H., An, Q.Q., Xu, T.T., Li, S.J., Liu, J.Y., Tao, N.N., et al. (2021). COVID-19 and tuberculosis coinfection: an overview of case reports/case series and meta-analysis. Front. Med. (Lausanne) *8*, 657006. https://doi.org/10.3389/fmed.2021.657006.
8. Leodolter, J., Warweg, J., and Weber-Ban, E. (2015). The Mycobacterium tuberculosis ClpP1P2 protease interacts asymmetrically with its ATPase partners ClpX and ClpC1. PLoS One *10*, e0125345. https://doi.org/10.1371/journal.pone.0125345.
9. Schmitz, K.R., and Sauer, R.T. (2014). Substrate delivery by the AAA+ ClpX and ClpC1 unfoldases activates the mycobacterial ClpP1P2 peptidase. Mol. Microbiol. *93*, 617–628. https://doi.org/10.1111/mmi.12694.
10. Trentini, D.B., Suskiewicz, M.J., Heuck, A., Kurzbauer, R., Deszcz, L., Mechtler, K., and Clausen, T. (2016). Arginine phosphorylation marks proteins for degradation by a Clp protease. Nature *539*, 48–53. https://doi.org/10.1038/nature20122.
11. Alhuwaider, A.A.H., and Dougan, D.A. (2017). AAA+ machines of protein destruction in mycobacteria. Front. Mol. Biosci. *4*, 49. https://doi.org/10.3389/fmolb.2017.00049.
12. Sauer, R.T., and Baker, T.A. (2011). AAA+ proteases: ATP-fueled machines of protein destruction. Annu. Rev. Biochem. *80*, 587–612. https://doi.org/10.1146/annurev-biochem-060408-172623.
13. Raju, R.M., Goldberg, A.L., and Rubin, E.J. (2012). Bacterial proteolytic complexes as therapeutic targets. Nat. Rev. Drug Discov. *11*, 777–789. https://doi.org/10.1038/nrd3846.
14. Gao, W., Kim, J.Y., Anderson, J.R., Akopian, T., Hong, S., Jin, Y.Y., Kandror, O., Kim, J.W., Lee, I.A., Lee, S.Y., et al. (2015). The cyclic peptide ecumicin targeting CLpC1 is active against Mycobacterium tuberculosis in vivo. Antimicrob. Agents Chemother. *59*, 880–889. https://doi.org/10.1128/AAC.04054-14.
15. Gavrish, E., Sit, C.S., Cao, S., Kandror, O., Spoering, A., Peoples, A., Ling, L., Fetterman, A., Hughes, D., Bissell, A., et al. (2014). Lassomycin, a ribosomally synthesized cyclic peptide, kills mycobacterium tuberculosis by targeting the ATP-dependent protease ClpC1P1P2. Chem. Biol. *21*, 509–518. https://doi.org/10.1016/j.chembiol.2014.01.014.
16. Zhang, S., Chen, J., Shi, W., Cui, P., Zhang, J., Cho, S., Zhang, W., and Zhang, Y. (2017). Mutation in clpC1 encoding an ATP-dependent ATPase involved in protein degradation is associated with pyrazinamide resistance in Mycobacterium tuberculosis. Emerg. Microbes Infect. *6*, e8. https://doi.org/10.1038/emi.2017.1.
17. Lupoli, T.J., Vaubourgeix, J., Burns-Huang, K., and Gold, B. (2018). Targeting the proteostasis network for mycobacterial drug discovery. ACS Infect. Dis. *4*, 478–498. https://doi.org/10.1021/acsinfecdis.7b00231.
18. Schmitt, E.K., Riwanto, M., Sambandamurthy, V., Roggo, S., Miault, C., Zwingelstein, C., Krastel, P., Noble, C., Beer, D., Rao, S.P., et al. (2011). The natural product cyclomarin kills Mycobacterium tuberculosis by targeting the ClpC1 subunit of the caseinolytic protease. Angew. Chem. Int. Ed. Engl. *50*, 5889–5891. https://doi.org/10.1002/anie.201101740.
19. Hawkins, P.M.E., Hoi, D.M., Cheung, C.Y., Wang, T., Quan, D., Sasi, V.M., Liu, D.Y., Linington, R.G., Jackson, C.J., Oehlers, S.H., et al. (2022). Potent bactericidal antimycobacterials targeting the chaperone ClpC1 based on the depsipeptide natural products ecumicin and Ohmyungsamycin A. J. Med. Chem. *65*, 4893–4908. https://doi.org/10.1021/acs.jmedchem.1c02122.
20. Brötz-Oesterhelt, H., Beyer, D., Kroll, H.P., Endermann, R., Ladel, C., Schroeder, W., Hinzen, B., Raddatz, S., Paulsen, H., Henninger, K., et al. (2005). Dysregulation of bacterial proteolytic machinery by a new class of antibiotics. Nat. Med. *11*, 1082–1087. https://doi.org/10.1038/nm1306.
21. Lee, B.G., Park, E.Y., Lee, K.E., Jeon, H., Sung, K.H., Paulsen, H., Rübsamen-Schaeff, H., Brötz-Oesterhelt, H., and Song, H.K. (2010). Structures of ClpP in complex with acyldepsipeptide antibiotics reveal its activation mechanism. Nat. Struct. Mol. Biol. *17*, 471–478. https://doi.org/10.1038/nsmb.1787.
22. Cobongela, S.Z.Z., Makatini, M.M., Mdluli, P.S., and Sibuyi, N.R.S. (2022). Acyldepsipeptide analogues: a future generation antibiotics for

tuberculosis treatment. Pharmaceutics *14*. https://doi.org/10.3390/pharmaceutics14091956.

23. Kazmaier, U., and Junk, L. (2021). Recent developments on the synthesis and bioactivity of ilamycins/rufomycins and cyclomarins, marine cyclopeptides that demonstrate anti-malaria and anti-tuberculosis activity. Mar. Drugs *19*. https://doi.org/10.3390/md19080446.
24. Vasudevan, D., Rao, S.P., and Noble, C.G. (2013). Structural basis of mycobacterial inhibition by cyclomarin A. J. Biol. Chem. *288*, 30883–30891. https://doi.org/10.1074/jbc.M113.493767.
25. Wolf, N.M., Lee, H., Zagal, D., Nam, J.W., Oh, D.C., Lee, H., Suh, J.W., Pauli, G.F., Cho, S., and Abad-Zapatero, C. (2020). Structure of the N-terminal domain of ClpC1 in complex with the antituberculosis natural product ecumicin reveals unique binding interactions. Acta Crystallogr. D Struct. Biol. *76*, 458–471. https://doi.org/10.1107/S2059798320004027.
26. Morreale, F.E., Kleine, S., Leodolter, J., Junker, S., Hoi, D.M., Ovchinnikov, S., Okun, A., Kley, J., Kurzbauer, R., Junk, L., et al. (2022). BacPROTACs mediate targeted protein degradation in bacteria. Cell *185*, 2338–2353. e18. https://doi.org/10.1016/j.cell.2022.05.009.
27. Maurer, M., Linder, D., Franke, K.B., Jäger, J., Taylor, G., Gloge, F., Gremer, S., Le Breton, L., Mayer, M.P., Weber-Ban, E., et al. (2019). Toxic activation of an AAA+ protease by the antibacterial drug cyclomarin A. Cell Chem. Biol. *26*, 1169–1179.e4. https://doi.org/10.1016/j.chembiol.2019.05.008.
28. Barbie, P., and Kazmaier, U. (2016). Total synthesis of cyclomarin A, a marine cycloheptapeptide with anti-tuberculosis and anti-malaria activity. Org. Lett. *18*, 204–207. https://doi.org/10.1021/acs.orglett.5b03292.
29. Junk, L., Schmiedel, V.M., Guha, S., Greb, P., Fischel, K., Rumpel, K., Kaur, P., Krishnamurthy, R.V., Narayanan, S., Kofink, C., et al. (2022). BacPROTAC-induced degradation of ClpC1 presents a novel anti-mycobacterial concept https://doi.org/10.26434/chemrxiv-2022-8hnrh.
30. Taylor, G., Frommherz, Y., Katikaridis, P., Layer, D., Sinning, I., Carroni, M., Weber-Ban, E., and Mogk, A. (2022). Antibacterial peptide CyclomarinA creates toxicity by deregulating the Mycobacterium tuberculosis ClpC1–ClpP1P2 protease. J. Biol. Chem. *298*, 102202. https://doi.org/10.1016/j.jbc.2022.102202.
31. Lo, J.H., Baker, T.A., and Sauer, R.T. (2001). Characterization of the N-terminal repeat domain of Escherichia coli ClpA—a class I Clp/HSP100 ATPase. Protein Sci. *10*, 551–559. https://doi.org/10.1110/ps.41401.
32. Hajdusits, B., Suskiewicz, M.J., Hundt, N., Meinhart, A., Kurzbauer, R., Leodolter, J., Kukura, P., and Clausen, T. (2021). Mcsb forms a gated kinase chamber to mark aberrant bacterial proteins for degradation. eLife *10*, 1–24. https://doi.org/10.7554/eLife.63505.
33. Suskiewicz, M.J., Hajdusits, B., Beveridge, R., Heuck, A., Vu, L.D., Kurzbauer, R., Hauer, K., Thoeny, V., Rumpel, K., Mechtler, K., et al. (2019). Structure of McsB, a protein kinase for regulated arginine phosphorylation. Nat. Chem. Biol. *15*, 510–518. https://doi.org/10.1038/s41589-019-0265-y.
34. Ogbonna, E.C., and Schmitz, K.R. (2021). Identification of diverse targets of arginine phosphorylation in Mycolicibacterium smegmatis by shotgun proteomics https://doi.org/10.1101/2021.04.05.438432.
35. Jumper, J., Evans, R., Pritzel, A., Green, T., Figurnov, M., Ronneberger, O., Tunyasuvunakool, K., Bates, R., Žídek, A., Potapenko, A., et al. (2021). Highly accurate protein structure prediction with AlphaFold. Nature *596*, 583–589. https://doi.org/10.1038/s41586-021-03819-2.
36. Harari, A., Zoltsman, G., Levin, T., and Rosenzweig, R. (2022). Hsp104 N-terminal domain interaction with substrates plays a regulatory role in protein disaggregation. FEBS Journal *289*, 5359–5377. https://doi.org/10.1111/febs.16441.
37. Lunge, A., Gupta, R., Choudhary, E., and Agarwal, N. (2020). The unfoldase ClpC1 of Mycobacterium tuberculosis regulates the expression of a distinct subset of proteins having intrinsically disordered termini. J. Biol. Chem. *295*, 9455–9473. https://doi.org/10.1074/jbc.RA120.013456.
38. Maniaci, C., Hughes, S.J., Testa, A., Chen, W., Lamont, D.J., Rocha, S., Alessi, D.R., Romeo, R., and Ciulli, A. (2017). Homo-PROTACs: bivalent small-molecule dimerizers of the VHL E3 ubiquitin ligase to induce self-degradation. Nat. Commun. *8*, 830. https://doi.org/10.1038/s41467-017-00954-1.
39. Domenech, P., and Reed, M.B. (2009). Rapid and spontaneous loss of phthiocerol dimycocerosate (PDIM) from Mycobacterium tuberculosis grown in vitro: implications for virulence studies. Microbiology (Reading) *155*, 3532–3543. https://doi.org/10.1099/mic.0.029199-0.
40. Andries, K., Verhasselt, P., Guillemont, J., Göhlmann, H.W., Neefs, J.M., Winkler, H., Van Gestel, J., Timmerman, P., Zhu, M., Lee, E., et al. (2005). A diarylquinoline drug active on the ATP synthase of Mycobacterium tuberculosis. Science *307*, 223–227. https://doi.org/10.1126/science.1106753.
41. Gengenbacher, M., Rao, S.P.S., Pethe, K., and Dick, T. (2010). Nutrient-starved, non-replicating Mycobacterium tuberculosis requires respiration, ATP synthase and isocitrate lyase for maintenance of ATP homeostasis and viability. Microbiology (Reading) *156*, 81–87. https://doi.org/10.1099/mic.0.033084-0.
42. Nguyen, T.V.A., Anthony, R.M., Bañuls, A.L., Nguyen, T.V.A., Vu, D.H., and Alffenaar, J.-W.C. (2018). Bedaquiline resistance: its emergence, mechanism, and prevention. Clin. Infect. Dis. *66*, 1625–1630. https://doi.org/10.1093/cid/cix992.
43. Mabhula, A., and Singh, V. (2019). Drug-resistance in Mycobacterium tuberculosis: where we Stand. MedChemComm *10*, 1342–1360. https://doi.org/10.1039/c9md00057g.
44. Ioerger, T.R., Feng, Y., Ganesula, K., Chen, X., Dobos, K.M., Fortune, S., Jacobs, W.R., Mizrahi, V., Parish, T., Rubin, E., et al. (2010). Variation among genome sequences of H37Rv strains of Mycobacterium tuberculosis from multiple laboratories. J. Bacteriol. *192*, 3645–3653. https://doi.org/10.1128/JB.00166-10.
45. Jain, P., Hsu, T., Arai, M., Biermann, K., Thaler, D.S., Nguyen, A., González, P.A., Tufariello, J.M., Kriakov, J., Chen, B., et al. (2014). Specialized transduction designed for precise high-throughput unmarked deletions in Mycobacterium tuberculosis. mBio *5*. e01245-14. https://doi.org/10.1128/mBio.01245-14.
46. Kiefer, A., Bader, C.D., Held, J., Esser, A., Rybniker, J., Empting, M., Müller, R., and Kazmaier, U. (2019). Synthesis of new cyclomarin derivatives and their biological evaluation towards Mycobacterium tuberculosis and Plasmodium falciparum. Chemistry *25*, 8894–8902. https://doi.org/10.1002/chem.201901640.
47. Beckham, K.S.H., Staack, S., Wilmanns, M., and Parret, A.H.A. (2020). The pMy vector series: a versatile cloning platform for the recombinant production of mycobacterial proteins in Mycobacterium smegmatis. Protein Sci. *29*, 2528–2537. https://doi.org/10.1002/pro.3962.
48. Parish, T., and Stoker, N.G. (2000). Use of a flexible cassette method to generate a double unmarked Mycobacterium tuberculosis tlyA plcABC mutant by gene replacement. Microbiology (Reading) *146*, 1969–1975. https://doi.org/10.1099/00221287-146-8-1969.
49. Neuhold, J., Radakovics, K., Lehner, A., Weissmann, F., Garcia, M.Q., Romero, M.C., Berrow, N.S., and Stolt-Bergner, P. (2020). GoldenBac: a simple, highly efficient, and widely applicable system for construction of multi-gene expression vectors for use with the baculovirus expression vector system. BMC Biotechnol. *20*, 26. https://doi.org/10.1186/s12896-020-00616-z.
50. Varadi, M., Anyango, S., Deshpande, M., Nair, S., Natassia, C., Yordanova, G., Yuan, D., Stroe, O., Wood, G., Laydon, A., et al. (2021). AlphaFold Protein Structure Database: massively expanding the structural coverage of protein-sequence space with high-accuracy models. Nucleic Acids Research *50*, D439–D444. https://doi.org/10.1093/nar/gkab1061.
51. Goddard, T.D., Huang, C.C., Meng, E.C., Pettersen, E.F., Couch, G.S., and Morris, J.H. (2018). UCSF ChimeraX: Meeting modern challenges in visualization and analysis. Protein Sci *27*, 14–25. https://doi.org/10.1002/pro.3235.

52. Emsley, P., Lohkamp, B., Scott, W.G., and Cowtan, K. (2010). Features and development of coot. Acta Crystallogr. D Biol. Crystallogr. *66*, 486–501. https://doi.org/10.1107/S0907444910007493.

53. Cox, J., Neuhauser, N., Michalski, A., Scheltema, R.A., and Olsen, J.V. (2011). Andromeda: a peptide search engine integrated into the MaxQuant environment. J Proteome Res *10*, 1794–1805. https://doi.org/10.1021/pr101065j.

54. Tyanova, S., Temu, T., Sinitcyn, P., Carlson, A., Hein, M.Y., Geiger, T., Mann, M., and Cox, J. (2016). The Perseus computational platform for comprehensive analysis of (prote)omics data. Nat. Methods *13*, 731–740. https://doi.org/10.1038/nmeth.3901.

55. Dorfer, V., Pichler, P., Stranzl, T., Stadlmann, J., Taus, T., Winkler, S., and Mechtler, K. (2014). MS Amanda, a universal identification algorithm optimized for high accuracy tandem mass spectra. J. Proteome Res. *13*, 3679–3684. https://doi.org/10.1021/pr500202e.

56. Käll, L., Canterbury, J.D., Weston, J., and Noble, W.S. (2007). Semi-supervised learning for peptide identification from shotgun proteomics datasets. Nat Methods *4*, 923–925. https://doi.org/10.1038/nmeth1113.

57. Afonine, P.V., Poon, B.K., Read, R.J., Sobolev, O.V., Terwilliger, T.C., and Urzhumtsev, A. (2018). Real-space refinement in PHENIX for cryo-EM and crystallography. Acta Crystallogr D Struct Biol *74*, 531–544. https://doi.org/10.1107/s2059798318006551.

58. Liebschner, D., Afonine, P.V., Baker, M.L., Bunkóczi, G., Chen, V.B., Croll, T.I., Hintze, B., Hung, L.W., Jain, S., McCoy, A.J., et al. (2019). Macromolecular structure determination using X-rays, neutrons and electrons: recent developments in Phenix. Acta Crystallogr. D Struct. Biol. *75*, 861–877. https://doi.org/10.1107/S2059798319011471.

59. Williams, C.J., Headd, J.J., Moriarty, N.W., Prisant, M.G., Videau, L.L., Deis, L.N., Verma, V., Keedy, D.A., Hintze, B.J., Chen, V.B., et al. (2018). MolProbity: more and better reference data for improved all-atom structure validation. Protein Sci. *27*, 293–315. https://doi.org/10.1002/pro.3330.

60. Kendall, S.L., and Frita, R. (2009). Construction of targeted mycobacterial mutants by homologous recombination. Methods Mol. Biol. *465*, 297–310. https://doi.org/10.1007/978-1-59745-207-6_20.

61. Belisle, J.T., Mahaffey, S.B., and Hill, P.J. (2009). Isolation of mycobacterium species genomic DNA. Methods Mol. Biol. *465*, 1–12. https://doi.org/10.1007/978-1-59745-207-6_1.

62. Goude, R., and Parish, T. (2008). Electroporation of mycobacteria. J. Vis. Exp., 761.

63. Schrodinger, LLC (2015). PhysiologyMOL molecular graphics system, version 1.8.

64. Hughes, C.S., Moggridge, S., Müller, T., Sorensen, P.H., Morin, G.B., and Krijgsveld, J. (2019). Single-pot, solid-phase-enhanced sample preparation for proteomics experiments. Nat. Protoc. *14*, 68–85. https://doi.org/10.1038/s41596-018-0082-x.

65. The, M., MacCoss, M.J., Noble, W.S., and Käll, L. (2016). Fast and accurate protein false discovery rates on large-scale proteomics data sets with Percolator 3.0. J. Am. Soc. Mass Spectrom. *27*, 1719–1727. https://doi.org/10.1007/s13361-016-1460-7.

66. Perez-Riverol, Y., Csordas, A., Bai, J., Bernal-Llinares, M., Hewapathirana, S., Kundu, D.J., Inuganti, A., Griss, J., Mayer, G., Eisenacher, M., et al. (2019). The PRIDE database and related tools and resources in 2019: improving support for quantification data. Nucleic Acids Res. *47*, D442–D450. https://doi.org/10.1093/nar/gky1106.

67. Sharma, V., Eckels, J., Schilling, B., Ludwig, C., Jaffe, J.D., MacCoss, M.J., and MacLean, B. (2018). Panorama public: a public repository for quantitative data sets processed in Skyline. Mol. Cell. Proteomics *17*, 1239–1244. https://doi.org/10.1074/mcp.RA117.000543.

68. Zweerink, S., Kallnik, V., Ninck, S., Nickel, S., Verheyen, J., Blum, M., Wagner, A., Feldmann, I., Sickmann, A., Albers, S.V., et al. (2017). Activity-based protein profiling as a robust method for enzyme identification and screening in extremophilic Archaea. Nat. Commun. *8*, 15352. https://doi.org/10.1038/ncomms15352.

69. Rehberg, N., Akone, H.S., Ioerger, T.R., Erlenkamp, G., Daletos, G., Gohlke, H., Proksch, P., and Kalscheuer, R. (2018). Chlorflavonin targets acetohydroxyacid synthase catalytic subunit IlvB1 for synergistic killing of Mycobacterium tuberculosis. ACS Infect. Dis. *4*, 123–134. https://doi.org/10.1021/acsinfecdis.7b00055.

STAR★METHODS

KEY RESOURCES TABLE

REAGENT or RESOURCE	SOURCE	IDENTIFIER
Bacterial and virus strains		
M. smegmatis mc^2-155	ATCC	ATCC 700084
M. smegmatis mc^2 155 ΔclpC2::gmR	This paper	N/A
M. smegmatis mc^2 155 ΔclpC3::gmR	This paper	N/A
M. smegmatis mc^2 155 ΔΔclpC2clpC3::gmR	This paper	N/A
M. smegmatis 607	DSMZ	ATCC 607, DSM 43465
M. tuberculosis H37Rv	William R. Jacobs Jr., Albert Einstein College of Medicine	H37RvMa (Ioerger et al.[44])
M. tuberculosis H37Rv ΔclpC2::hygR	This paper	N/A
ΦphAE159	Jain et al.[45]	N/A
Chemicals, peptides, and recombinant proteins		
M. smegmatis ClpC1	Morreale et al.[26]	N/A
M. smegmatis ClpC1^{DWB}	This paper	N/A
M. smegmatis ClpC1$^{DWB\text{-}F444A}$	This paper	N/A
M. smegmatis ClpC1 NTD (1–148)	Morreale et al.[26]	N/A
M. smegmatis ClpP1 with his-tag	Morreale et al.[26]	N/A
M. smegmatis ClpP2 with his-tag	Morreale et al.[26]	N/A
M. smegmatis ClpC2 with his-tag	This paper	N/A
M. smegmatis ClpC2^{CRD} with his-tag	This paper	N/A
M. smegmatis ClpC3 with his-tag	This paper	N/A
BRDT$_{BD1}$-NrdI	Morreale et al.[26]	N/A
α-casein	Sigma-Aldrich	Cat#C6780-5G
β-casein	Sigma-Aldrich	Cat#C6905-1G
Pyruvate kinase	Sigma-Aldrich	Cat#9136-5KU
Lactic dehydrogenase	Sigma-Aldrich	Cat#1254-5KU
NADH	Roche	10128023001
Phosphoenolpyruvate	Sigma-Aldrich	Cat#860077-1G
pArg-JQ1	This paper	N/A
dCym-JQ1	This paper	N/A
Homo-BacPROTAC6	Junk et al.[29]	N/A
Homo-BacPROTAC6dis	Junk et al.[29]	N/A
dCym6	Junk et al.[29]	N/A
dCym6dis	Junk et al.[29]	N/A
Homo-BacPROTAC7	Junk et al.[29]	N/A
Homo-BacPROTAC7dis	Junk et al. [29]	N/A
dCym7	Junk et al.[29]	N/A
dCym7dis	Junk et al.[29]	N/A
dCym	Barbie and Kazmaier[28]	N/A
dCymM	Kiefer et al.[46]	N/A
Ecu* (analogue 6)	Hawkins et al.[19]	N/A
Ecu**	This paper	N/A
LVAWG peptide	This paper	N/A
TCEP	Sigma-Aldrich	Cat#C4706-10G
Tween80	Sigma-Aldrich	Cat# P1754-500ML
Tween20	Sigma-Aldrich	Cat#P9416-100ML

(*Continued on next page*)

Continued

REAGENT or RESOURCE	SOURCE	IDENTIFIER
Streptavidin	Prospec	
cOmplete, EDTA-free Protease inhibitor cocktail	Roche	05056489001
Trypsin	Promega	V5280
BXT buffer	Iba lifescience	Cat#2-1042-025
Trifluoroacetic Acid	Fisher Scientific	Cat#11378277
Acetonitrile	Merck	Cat#113212
Formic acid	Sigma-Aldrich	27001-1L-M
Iodacetamide	Sigma-Aldrich	Cat#L6125-25G
Bedaquiline	MedChemExpress	HY-14881
Ethambutol	Sigma-Aldrich	E4630
SDC	Sigma-Aldrich	Cat#30970-100G
Middlebrook 7H9 Broth Base	Sigma-Aldrich	M0178-500G
BD Difco Middlebrook 7H10 Agar	Fisher Scientific	DF0627-17-4
HBS-P+ buffer 10x	Cytiva	Cat#BR100671
Critical commercial assays		
High Sensitivity DNA Kit	Agilent Technologies, Inc.	Cat#5067-4626
TruePrep DNA Library Prep Kit V2 for Illumina	Vazyme Biotech Co.	Cat#TD501
EZ-Link™ NHS-PEG4 Biotinylation Kit	Thermo Fisher Scientific	Cat#21455
Amine-coupling kit	Cytiva	Cat#BR100050
Deposited data		
Msm $ClpC2_{CRD}$:pArg Crystal Structure	This paper and Protein Data Bank (PDB)	8B9O
Mtb $ClpC1_{NTD}$:Ecu** Crystal Structure	This paper and Protein Data Bank (PDB)	8B9U
Msm IP-MS proteomics Data of ClpC2 interactome	This paper and PRoteomics IDentification Database	PXD037231
Msm LFQ proteomics Data of dCym/Ecu* treatment (10 μM)	This paper and PRoteomics IDentification Database	PXD037232
Msm LFQ proteomics Data of dCym treatment (150 μM)	This paper and PRoteomics IDentification Database	PXD037234
Msm LFQ proteomics Data of BacPROTAC treatment	This paper and PRoteomics IDentification Database	PXD037235
Msm MS-PRM Data	This paper, PanoramaWeb and PRoteomics IDentification Database	PXD037198
Mtb IP-MS proteomics Data of dCym derivative targets	This paper and PRoteomics IDentification Database	PXD037712
Mtb LFQ proteomics Data of BacPROTAC treatment	This paper and PRoteomics IDentification Database	PXD037730
Oligonucleotides		
Primers for generation of *M. smegmatis* genomic mutants, see Table S5	This paper	N/A
Primers for generation of *M. tuberculosis ΔclpC2*, see Table S5	This paper	N/A
Primers for construction of plasmids for inducible expression in mycobacteria, see Table S5	This paper	N/A
Recombinant DNA		
pET-21a (+) plasmid	Addgene	https://www.addgene.org/
pMyC plasmid	Beckham et al.[47]	RRID:Addgene_42192
p2NIL plasmid	Parish and Stoker[48]	RRID:Addgene_20188

(*Continued on next page*)

Continued

REAGENT or RESOURCE	SOURCE	IDENTIFIER
pGOAL19 plasmid	Parish and Stoker[48]	RRID:Addgene_20190
p0004S	Jain et al.[45]	N/A
pGB-Dest	Neuhold et al.[49]	N/A
Software and algorithms		
AlphaFold	Jumper et al.[35], Varadi et al., 2022[50]	N/A
UCSF Chimera-X	Goddard et al., 2018[51]	https://www.cgl.ucsf.edu/chimerax/
PyMol	The PyMOL Molecular Graphics System, Version 2.0 Schrödinger, LLC	https://pymol.org/2/ (Continued)
Coot	Emsley et al.[52]	https://www2.mrc-lmb.cam.ac.uk/personal/pemsley/coot/
Python 3	Python	https://www.python.org/
RStudio	RStudio	https://www.rstudio.com/
Proteome Discoverer 2.5	Thermo Fisher Scientific	N/A
MaxQuant 2.1	Cox et al., 2011[53]	https://www.maxquant.org/maxquant/
Perseus 1.6	Tyanova et al.[54]	https://www.maxquant.org/perseus/
Cassiopeia	N/A	https://github.com/moritzmadern/Cassiopeia_LFQ
MS Amanda	Dorfer et al.[55]	https://ms.imp.ac.at/
Percolator	Kall et al., 2007[56]	N/A
Biacore Insight Evaluation	N/A	N/A
Geneious	N/A	https://www.geneious.com/
Phenix	Afonine et al., 2018[57], Liebschner et al.[58]	https://phenix-online.org/
MolProbity	Williams et al.[59]	http://molprobity.biochem.duke.edu/ N/A
Prism	GraphPad	https://www.graphpad.com/scientific-software/prism
Other		
Cu/Pd Hexagonal 400 mesh grids	Agar	Cat#AGG2440PD
Nunc™ MicroWell™ 96-Well, Nunclon Delta- Treated, Flat-Bottom Microplate	Fisher Scientific	Cat#167008
U-shaped 96-well glass-coated microplates	Fisher Scientific	Cat#60180-P300
flat 96-well plates Thermo Nunc Microwell	Sigma-Aldrich Fisher	Cat#P8366-50EA
U-shaped 96-well glass-coated microplates Sera-Mag	Fisher Scientific	Cat#60180-P306
Sera-Mag SpeedBeads, variant 1	Cytvia	Cat#45152105050250
Sera-Mag SpeedBeads, variant 2	Cytvia	Cat#65152105050250
PepSwift Monolithic RSLC column	Thermo Fisher Scientific	Cat#164542
XBridge Peptide BEH C18 Column Acclaim	Waters	Cat#186003613
Acclaim PepMap C-18 precolumn	Thermo Fisher Scientific	Cat#160454
Acclaim PepMap C-18 column	Thermo Fisher Scientific	Cat#164942
Eclipse XDB-C18 (5 mm)	Agilent	Cat#990967-902
Pierce™ Avidin Agarose beads	Thermo Fisher Scientific	Cat#20219
Glass microfiber tips	GE Healthcare	Cat#1822-024
Strep-Tactin® Sepharose® resin	Iba lifescience	Cat#2-1201-025
Series S Sensor chip CM5	Cytiva	Cat#29149603
Series S Sensor chip NTA	Cytiva	Cat#BR100532
Zeba™ Spin Desalting Columns, Plates, and Cartridges, 7K MWCO, 0.5–100 mL	Thermo Fisher Scientific	Cat#89882

RESOURCE AVAILABILITY

Lead contact

Further information and requests for resources and reagents should be directed to and will be fulfilled by the lead contact, Tim Clausen (tim.clausen@imp.ac.at).

Materials availability

All unique materials and reagents generated in this study are available from the lead contact with a completed material transfer agreement. There are restrictions to the availability of the generated BacPROTAC probes and simplified cyclomarin analogues generated in this study due to a limited stock. Reasonable aliquots of the compounds are available until stocks run out from the lead contact with a completed material transfer agreement.

Data and code availability

Coordinates of the $ClpC2_{CRD}$:pArg and the $ClpC1_{NTD}$:Ecu** crystal structures have been deposited at the Protein Data Bank (PDBe) under the accession codes 8B9O and 8B9U. The mass spectrometry proteomics data have been deposited to the ProteomeXchange Consortium via the PRIDE partner repository with the dataset identifier PXD037231, PXD037232, PXD037234, PXD037235, PXD037712 and PXD037730. PRM data has been submitted to PRIDE as well as to PanoramaWeb (PXD037198). The paper does not report original code. Any additional information required to reanalyze the data reported in this paper is available from the lead contact upon request.

EXPERIMENTAL MODEL AND SUBJECT DETAILS

M. smegmatis mc^2-155 (ATCC 7000084) was directly purchased from ATCC and freshly inoculated from glycerol stock. *M. smegmatis* strain ATCC 607 was purchased from DSMZ (DSM 43465) and freshly inoculated from a plate. *M. tuberculosis* H37Rv was obtained from William R. Jacobs Jr. (Albert Einstein College of Medicine) and freshly inoculated from glycerol stock. The genomic knockout strains of *M. smegmatis* mc^2 155 *ΔclpC2::gmR*, *ΔclpC3::gmR*, and *ΔΔclpC2clpC3::gmR* were obtained after homologous recombination using the p2NIL/pGOAL[48] (Addgene plasmid #20188; https://www.addgene.org/20188/; RRID:Addgene_20188 and Addgene plasmid #20190; https://www.addgene.org/20190/; RRID:Addgene_20190) system adapted from Kendall et al[60] as described below and apart from the site of recombination can be considered isogenic to the parental strain. *M. tuberculosis ΔclpC2::hygR* was obtained via specialized phage transduction and apart from the site of integration can be considered isogenic to the parental strain.

Liquid cultures of all strains of *M. smegmatis* mc^2 155 were inoculated with 5 μl of a glycerol stock (OD_{600} 0.5) into in Middlebrook 7H9 medium (Sigma) supplemented with 0.2% (v/v) glycerol and 0.025% (v/v) Tween80 (Sigma) and respective antibiotics if applicable. That is, *M. smegmatis* transformed with the respective pMyC vectors were additionally supplemented with 50 μg/ml Hygromycin and 1 μg/ml Gentamicin was added for the knockout mutants. Constant agitation at 37 °C was applied and main cultures were inoculated out of exponential growing overnight cultures. If applicable, ectopic expression was induced with 0.1% (w/v) acetamide. Cells were harvested by centrifugation (3,000 x g, 5 min, 25 °C) and processed according to the respective experiment. *M. smegmatis* strain ATCC 607 was cultivated as described above except that the medium was supplemented with 0.1% (v/v) glycerol. Solidified medium was prepared using Middlebrook 7H10 agar (Difco) supplemented with 0.5% (v/v) glycerol. MIC assay plates for overexpression strains were supplemented with 0.1% (w/v) acetamide and 50 μg/ml Hygromycin. All plates were incubated for 2.5-5 days at 37 °C. *M. tuberculosis* was grown aerobically at 37 °C in Middlebrook 7H9 liquid media supplemented with 10% DS (2% (w/v) glucose; 0.085% (w/v) sodium chloride), 0.5% (v/v) glycerol and 0.025% (v/v) Tween 80. Solidified medium for *Mtb* was supplemented with 10% ADS (5% (w/v) bovine serum albumin; 2% (w/v) glucose; 0.085% (w/v) sodium chloride) and 0.5% (v/v) glycerol. For the *ΔclpC2* gene deletion mutant, hygromycin was added to a final concentration of 50 μg/ml.

METHOD DETAILS

Isolation of chromosomal DNA

Mycobacterial chromosomal DNA was isolated using an adapted protocol derived from Belisle et al.[61] In short, exponentially growing cells of *M. smegmatis* mc^2 155 were harvested at OD 1.5 by centrifugation for 15 min, 3000 x g, 4 °C. Cells were subsequently washed with TE (10 mM Tris/HCl, pH 8.0, 1 mM EDTA) and the final cell pellet was weighed resulting in 600 mg wet weight. To initiate the isolation, cells were frozen overnight at -80 °C. Subsequently, the thawed pellet was dissolved in 500 μl TE and incubated for 60 minutes with equal volumes of Chloroform:methanol (2:1) (20 °C, 600 rpm shaking with Thermo rocker). Aqueous and organic phase were separated at 2,500 x g for 20 minutes and both phases were carefully removed by pipetting before the tube was dried at 55 °C for 15 min. 375 μl TE were added and the suspension was rigorously dissolved by vortexing. pH was increased to 9.0 and lysis was initiated by adding 0.01 x vol lysozyme (sigma) and incubation at 37 °C for 12 hours. Interfering proteins were handled by adding 0.2 x vol 10% SDS, 0.02 x vol Proteinase K (VWR) and incubation for six hours at 55 °C. Extraction of DNA was performed at room temperature and started by adding an equal volume of phenol/chloroform/isoamylalcohol (25:24:1) for 30 minutes. The

aqueous layer was transferred into a new tube and phenol was washed out by adding an equal volume of chloroform:isoamyl alcohol (24:1) for ten minutes and subsequent centrifugation for 30 min, 12000 x g. To remove waxy polar lipids and to precipitate the DNA, 0.1 x vol 3 M sodium acetate pH 5.2 and 1 x vol isopropanol were added to the clean aqueous phase. The suspension was incubated for 60 minutes at 4 °C before the DNA was fished and winded up with a pipet tip to transfer it into a new tube. Subsequently, the DNA was washed with ice cold (-20 °C) ethanol, centrifuged and ethanol was left to evaporate. Finally, the DNA was dissolved in 100 μl nuclease free water and concentration was measured with DeNovix DS-11 FX+ Spectrophotometer, at the same time checking sufficient purity of the DNA with 260/280 and 260/230 ratio. This procedure resulted in 1.2 μg/μl DNA which was used as template for PCR.

Construction of mycobacterial mutants

The genomic knockout strains of *M. smegmatis* mc^2 155 *ΔclpC2::gmR*, *ΔclpC3::gmR*, and *ΔΔclpC2clpC3::gmR* were constructed via homologous recombination using the p2NIL/pGOAL system adapted from.[60] Briefly, a fusion product, which consists of (i) upstream *clpC2* or *clpC3* homologous region, amplified from freshly isolated mycobacterial chromosomal DNA (mycobacterial DNA was isolated from a late-exponential growth phase culture with an in-house protocol adapted from,[61] see supplemental information, (ii) Kanamycin promotor amplified from p2NIL, (iii) Gentamicin resistance cassette amplified from pGB-Dest,[49] (iv) Kanamycin terminator amplified from p2NIL, and (v) downstream *clpC2* or *clpC3* homologous region amplified from mycobacterial chromosomal DNA was ligated via Gibson assembly into the p2NIL plasmid, and transformed into *E. coli* XL10 Gold. The plasmid *p2NIL-clpC2/3HRup-Kanprom-gmR-Kanterm-clpC2/3HRdown* was ligated with antibiotic cassette 19 from pGOAL19, again transforming into *E. coli* XL10 Gold. The final plasmid was verified by sequencing and transformed into *M. smegmatis* mc^2 155 via electroporation. Preparation of competent cells and electroporation was performed according to.[62] Successful double crossover mutants were verified by sequencing and PRM. All primer sequences are listed in Table S5. To generate *M. smegmatis* mc^2 155 *ΔΔclpC2clpC3::gmR*, electrocompetent cells of *M. smegmatis* mc^2 155 *ΔclpC3::gmR* were transformed with *p2NIL-cas19-clpC2HRup-Kanprom-gmR-Kanterm-clpC2HRdown* to initiate the crossover events.

Rv2667 (=*clpC2*) gene disruption in *Mtb* strain H37Rv was achieved employing specialized transduction.[45] Briefly, an allelic exchange substrate was designed to replace *clpC2* in *Mtb* with a γδ*res-sacB-hyg*-γδ*res* cassette comprising a *sacB* as well as a hygromycin resistance gene flanked by *res*-sites of the γδ-resolvase. Upstream and downstream flanking regions of the *clpC2* gene were amplified by PCR using primers listed in Table S5. Subsequently, the flanking regions were digested with the indicated restriction enzymes and ligated with the *Van91*I-digested p0004S vector.[45] The resulting allelic exchange plasmid was then linearized with *PacI*, cloned, and packaged into the temperature-sensitive phage ΦphAE159,[45] yielding knock-out phages that were propagated in *Msm* at 30 °C. Allelic exchange in *Mtb* was achieved by specialized transduction at the non-permissive temperature of 37 °C, using hygromycin for selection, resulting in gene deletion and replacement by γδ*res-sacB-hyg*-γδ*res* cassette. Obtained hygromycin-resistant transductants were screened for correct gene disruption by diagnostic PCR analysis.

Cloning of overexpression constructs

For overexpression of *clpC2* and *clpC3*, the respective construct was inserted into pMyC[47] (pMyC was a gift from Annabel Parret & Matthias Wilmanns (Addgene plasmid #42192; http://n2t.net/addgene:42192; RRID:Addgene_42192)) via Gibson assembly, using isolated chromosomal DNA as template for insert PCR. ClpC2 was cloned either with a C-terminal 8xHis tag (for MIC assays) or a C-terminal twinstrep tag (for IP) and ClpC3 was cloned with a C-terminal 6xHis tag. All primer sequences are listed in Table S5. The Gibson assembly products were transformed into *E. coli* XL10 Gold and verified by sequencing. For ectopic overexpression, the respective construct was transformed in *M. smegmatis* mc^2 155 as described.[62]

Protein expression and purification

Plasmids for expression in *E. coli* were transformed in BL21 (DE3) cells (ClpC2 His6, ClpC2-CTD His6 and ClpC3 His6 on pET21a vector) or Rosetta (DE3) cells (ClpC1, ClpC1^{DWB}, ClpP1 His4, ClpP2 His4) and grown in LB medium containing the respective antibiotics at 37 °C. Protein expression was induced upon addition of 0.5 mM isopropyl-1-thio-β-D-galactopyranoside (IPTG) at an OD_{600} of 0.8. Subsequently, the temperature was reduced to 21 °C and cell growth resumed overnight. Cells were harvested by centrifugation and lysed by sonication in purification buffer A (50 mM HEPES-NaOH pH 7.5, 75 mM KCl, 2 mM ETDA and 10% (v/v) glycerol) supplemented with protease inhibitor and benzonase. The lysate was cleared by centrifugation followed by filtration of the supernatant (0.2 μm).

For purification of ClpC1 (and ClpC1^{DWB}), the cell pellet was suspended in buffer A. ClpC1 was precipitated from cleared supernatant at 40% (w/v) ammonium sulfate at 4 °C overnight and collected by centrifugation. ClpC1 was resuspended in buffer A and loaded on an anion exchange column (HiLoad 26/10 Q Sepharose column, GE Healthcare) equilibrated by buffer A. The column was washed to baseline absorbance and ClpC1 was eluted in a gradient to 1 M KCl. Pure fractions were pooled, concentrated, and loaded on a size exclusion chromatography (SEC) column (HiLoad, Superdex 200 16/60, GE Healthcare), equilibrated with buffer C, containing 50 mM HEPES-NaOH pH 7.5, 150 mM KCl and 10% (v/v) glycerol. Purification was monitored for homogeneity by Coomassie stained SDS-PAGE. Fractions containing ClpC1 were pooled and concentrated before flash freezing in liquid nitrogen and stored at -80 °C.

For purification of ClpP1 or ClpP2, cells were suspended in buffer B, containing 50 mM HEPES-NaOH pH 7.5, 500 mM KCl and 1 mM TCEP. Cleared lysates were applied to a 5 ml agarose HisTrap column (GE Healthcare) equilibrated with buffer B, the column was washed with additional 50 mM and later 75 mM imidazole. Bound proteins were eluted in a gradient to 250 mM imidazole. Pure fractions were pooled and concentrated for application to SEC (Superdex 200 16/60, GE Healthcare) equilibrated with buffer C containing 50 mM HEPES-NaOH pH=7.5, 150 mM KCl with additional 1 mM TCEP. Purification of ClpC2, ClpC2-CTD or ClpC3 followed the identical protocol, except that buffer B contained 50 mM HEPES-NaOH pH=7.5, 150 mM NaCl, and buffer B contained 50 mM HEPES-NaOH pH=7.5, 150 mM NaCl. Pure fractions were pooled after SEC, concentrated and aliquots were flash frozen in liquid nitrogen, before storage at -80 °C. Processing of full-length ClpP1 and ClpP2 to the mature ClpP1P2 complex was performed as previously described.[8]

Surface plasmon resonance (SPR)

For potent binders (KD < 1 μM), the ClpC1-NTD from *M. tuberculosis* and ClpC2 from *M. smegmatis* were chemically biotinylated using the EZ-Link NHS-PEG4-Biotin kit (Thermo Scientific) according to the manufacturer's instructions. The following modifications were made: The reaction was incubated for three hours, agitating at RT with a molar ratio of 1:5 between biotin reagent and protein in 10 mM HEPES, pH 7.4, 0.05% (v/v) Tween20, 150 mM NaCl (HBS-P+, Cytiva). Zeba Spin desalting columns (Thermo Scientific) were subsequently used to get rid of non-reacted NHS-PEG4-Biotin. Streptavidin (Prospec) was immobilized to a density of 2000-3000 RUs onto all flow cells of a CM5 chip (Cytiva) at 25 °C, in 10 mM sodium acetate pH 5.0 using the amine-coupling kit (Cytiva). Biotinylated ClpC1-NTD and ClpC2 were captured to flow cells 2 and 3. ClpC3 from *M. smegmatis* was captured and coupled via its His6-tag onto flow cell 4 of a NTA chip (Cytiva), which was preloaded (Ni^{2+}) and activated with EDC/NHS according to the manufacturer's instructions. For all three, capture-coupling was performed in HPS-P+ at 25 °C up to a density of 100-500 RUs. Similarly, for weak binders (KD > 1 μM), ClpC1-NTD, ClpC2 and ClpC3 were capture coupled onto flow cells 2, 3 and 4 of a NTA chip, respectively, to a density of 1200 – 2000 RUs. The binding of the compounds was subsequently measured on a Biacore T200 instrument (Cytiva) at 25 °C in 25 mM Tris(hydroxymethyl)aminomethane, pH 7.5, 150 mM NaCl, 1% (v/v) DMSO, 0.01% (v/v) Tween20, in two different protocols depending on the binding potency of the compounds measured. At least three independent measurements were performed for each compound with mean values reported. For potent binders, sensorgrams were recorded at five different compound concentrations in single-cycle mode, at a flow rate of 100 μl/min, 20 s contact time and 600 s dissociation time. dCym served as positive control. Weak binders were measured in multi-cycle mode, at nine concentrations and a flow rate of 30 μl/min, 60 s contact time and 600 s dissociation time. As a positive control, phosphoarginine was used. Sensorgrams were double referenced prior to data analysis using Biacore Insight Evaluation Software. Data were fitted using the 1:1 interaction model with a term for mass-transport included. Single-cycle data were fitted kinetically. For multi-cycle data, steady state affinity fits were used. K_D values are reported in Table S2. Representative sensorgrams and fits are shown in Data S1A.

Analytical size exclusion chromatography (aSEC)

For size exclusion runs, 25 μM $ClpC1^{DWB}$ (inactive ATPase mutant, capable of binding, but not hydrolyzing ATP and stabilized in its hexameric state) or $ClpC1^{DWB\text{-}F444A}$ was premixed together with equimolar levels of dCym or DMSO (%) in running buffer (50 mM Tris pH 7.5, 100 mM NaCl, 5 mM $MgCl_2$ and 0.5 mM ATP). Samples were loaded using a 30 μL loop on a Superose 6 3.2/300 increase column (GE healthcare), previously equilibrated in running buffer. Runs were performed at room temperature at a 0.05 mL/minute flow rate. 100 μL fractions were collected for grid preparation for further electron microscopy analysis.

Negative staining EM

In the presence of dCym, $ClpC1^{DWB}$ elutes at higher molecular weights in a second peak earlier than the ClpC1 hexameric peak. Fractions covering this elution volume were selected for $ClpC1^{DWB}$ and $ClpC1^{DWB\text{-}F444A}$ previously incubated with dCym or DMSO. Grids were prepared with glow-discharged carbon-coated Cu/Pd Hexagonal 400 mesh grids (Agar Scientific) using 5 μl protein sample and stained with a solution of 2% uranyl acetate. The grids were screened and then imaged on a Morgagni microscope equipped with a Morada camera (Olympus-SIS) using a pixel size of 4.7 Å/px.

In vitro substrate degradation assay

The effect of dCym and Ecu* on α-casein and β-casein degradation by mycobacterial ClpC1P1P2 was tested using *in vitro* degradation assays. Hexameric *M. smegmatis* ClpC1 (0.5 μM) together with mature (14-mer complex after pro-peptide cleavage) *M. smegmatis* ClpP1P2 (0.3 μM) was incubated shortly with either 100 μM Ecu* (in DMSO), dCym (in DMSO) or DMSO as control. A final DMSO concentration of 1% was used for all conditions. The assay was set up using 15 μM substrate (α-casein or ß-casein), 20 mM phosphoenolpyruvate (PEP) and 10 U/ml pyruvate kinase (Sigma Aldrich) in a buffer containing 50 mM HEPES pH 7.5, 100 mM KCl, 10 mM $MgCl_2$ and 10% (v/v) glycerol. To start the reaction, ATP was added to a final concentration of 5 mM and the reaction was incubated at 37 °C. Timepoints of 5 μl were taken before reaction start and then after 10, 20 and 45 minutes. To stop the reaction, SDS sample buffer was added prior to an SDS-PAGE and Coomassie staining. To test competition for ß-casein binding of ClpC2 and ClpC1, ClpC2-CTD equimolar to ClpC1 was added to the degradation assay, without using compound or DMSO.

In addition, to test *in vitro* competition for substrate binding of ClpC2 and ClpC1, the pArg-JQ1 and dCym-JQ1 treatment was carried out using ClpC2 at levels equimolar and in 4x excess to ClpC1. Here, ClpC1, ClpP1P2 and ClpC2 were incubated together with

100 μM compound with $BRDT_{BD1}$-NrdI as substrate (the attached NrdI represents a physiological *B. subtilis* ClpC substrate), while the assay was otherwise carried out as described above.

To account for solubility issues of HBPs, the final reactions contained 1.5 μM substrate protein *M. tuberculosis* ClpC1-NTD, 15 mM PEP and 40 mM $MgCl_2$ in the assay buffer. All other conditions were kept as described above.

In vitro ClpC2 pulldown

Substrate binding to ClpC2 and occupation of the conserved hydrophobic pocket was tested by performing a pulldown of 15 μM ClpC2-His using Ni-NTA agarose beads (Qiagen), together with equal concentrations of the substrates α-casein and β-casein in a buffer containing 50 mM HEPES pH 7.5 and 100 mM KCl. As control, empty beads were incubated with substrate alone. The sample was washed three times with the same buffer containing 25 μM imidazole. To test competition of substrate and antibiotics for the same binding site, after incubation of ClpC2 with substrate, 25 μM dCym was added. His-tagged ClpC2 (and controls) was eluted from the beads by addition of 250 μM imidazole and the samples were subsequently evaluated via SDS-PAGE.

Co-crystallization and structure determination

Purified ClpC2-CTD at a concentration of 15 mg/mL and supplemented with 100 mM pArg was crystallized using a reservoir solution containing 12.5% (w/v) PEG 1000, 12.5% (w/v) PEG 3350, 12.5% (v/v) MPD, 0.02 M of each amino acid and 0.1 M MES/imidazole pH 6.5. Crystals were grown at room temperature, directly harvested and flash-cooled in liquid nitrogen. Diffraction data at a resolution of 2.0 Å were collected at the beamline P11 at DESY (Hamburg, Germany). ClpC1-NTD was purified as previously described.[26] Purified ClpC1-NTD at a concentration of 15 mg/mL and supplemented with 1 mM of Ecu** was crystallized using a reservoir solution containing 10 mM Tris-HCl pH 7.5 and 3.1 M sodium formate. Crystals were grown at room temperature transferred into the reservoir solution supplemented with additional 20 % (v/v) glycerol and flash-cooled in liquid nitrogen. Diffraction data at a resolution of 2.25 Å were collected at an in-house X-ray source. Initial phases were obtained by Molecular Replacement using PHASER and the structure of $ClpC1_{NTD}$ (PDB: 3WDB)[24] as starting model. The model was improved in iterative cycles of manual building using Coot[52] and refinement with Phenix,[58] omitting 5% of randomly selected reflections for calculation of Rfree. Model quality was monitored using MolProbity[59] and the final model exhibited good stereochemistry (Table S3). Structural illustrations were made using PYMOL.[63]

M. smegmatis sample preparation for MS analysis

Exponentially growing cells as described in the experimental models section were harvested by centrifugation at and concentrated to an OD_{600} of 5 in fresh 7H9 medium. 750 μL aliquots were transferred into each well of a 24-well glass-coated microplate (WebSeal Plate+, Thermo Scientific) and treated with either 15 μl DMSO or 15 μl of a 1 mM dCym or Ecu* stock (to achieve a final concentration of 10 μM compound and 1% DMSO per well). Subsequently, another 750 μl cell culture was added to ensure proper mixing of the compound. Each treatment was performed in triplicates. Before treatment, after 30 minutes incubation and after 120 minutes incubation, 250 μL of cell suspension was harvested from each well, and the resulting pellets were flash-frozen in liquid nitrogen. Prior to cell lysis, pellets were thawed, resuspended in 100 μL lysis buffer (50 mM HEPES pH 7.2, 150 mM KCl) and lysed for 10 minutes using a Bioruptor (Diagenode, 10 cycles, 30 seconds on - 30 seconds off) after adding a small amount of glass beads. The lysates were clarified by centrifugation (10 minutes, 4 °C, 20,000 x g), flash-frozen and stored at -80 °C.

For the treatment of *M. smegmatis* mc^2 155 WT and *ΔclpC2::gmR* with higher compound concentration, a culture volume of 600 μl at OD_{600} of ~5 (300 μl + 300 μl) was incubated with a final concentration of 150 μM dCym or DMSO (final concentration = 1%). 250 μl were collected before treatment, after two hours and six hours and processed as described above.

For intracellular degradation proteomics, *M. smegmatis* strain ATCC™ 607™ was used. A final concentration of 12.5 μM HomoBacPROTAC was applied for treatment. For the intracellular degradation assay, 100 μl concentrated cell suspension (concentrated by factor 5) were incubated for 24 hours. To harvest the cells, 90 μl cell suspension from each well was centrifuged at 4,000 x g and 23 °C for 3 min, resuspended in 100 μl cold lysis buffer (50 mM HEPES pH 7.5, 150 mM KCl, 10% glycerol (v/v)) containing complete protease inhibitor cocktail (EDTA-free, Roche) and stored on ice until lysis. Cells were lysed in a Bioruptor Pico and centrifuged at 21,000 x g and 4 °C for 30 min. The supernatant was flash frozen in liquid nitrogen and stored at -80 °C.

Whole cell proteomics & PRM sample preparation

Cleared lysates were processed according to the single-pot SP3 protocol[64] for low input proteomics sample preparation. Each lysate of 100 μl was reduced with 10 mM dithiothreitol (DTT, Sigma Aldrich) for 45 minutes at 37 °C and subsequently alkylated with 20 mM iodoacetamide (IAA, Sigma Aldrich) at room temperature for 60 minutes. In parallel, a 1:1 mixture of 50 mg/mL Sera-Mag SpeedBeads (GE Healthcare, cat. no. 45152105050250) and 50 mg/mL Sera-Mag SpeedBeads (GE Healthcare, cat. no. 65152105050250), exhibiting different surface hydrophilicity, was washed, and prepared in water. To each lysate, 15 μL of the prepared SP3 bead stock was added and binding was induced by the addition of 100 μL ethanol. To ensure proper binding, samples were incubated on a shaker for five minutes at 24 °C and 1000 rpm. After protein binding, beads were washed three times with 200 μL rinsing solution (80% ethanol in water) while being kept on a magnetic rack. Protein elution from the beads was enforced by addition of 100 mM ammonium bicarbonate buffer (pH = 8.5, Sigma Aldrich). To disaggregate the beads, the tubes were shortly sonicated in a

water bath. For protein digestion, 1:25 wt/wt ratio of trypsin to protein was added and the samples were incubated overnight at 37 °C in a thermo-shaker at 1000 rpm. Finally, 5% TFA was used to adjust the pH to 3, prior to MS analysis.

Immunoprecipitation (IP) sample preparation

Cultures of *M. smegmatis* mc^2-155 cell lines *ΔclpC2:ev* and *ΔclpC2*:ClpC2^{twinstrep} as described in the cloning and cultivation section were harvested by centrifugation, the pellet was taken up in 500 µl buffer (50 mM HEPES pH 7.2, 100 mM KCl) and subsequently lysed for 10 minutes using a Bioruptor (Diagenode, 10 cycles, 30 seconds on - 30 seconds off) after adding a small amounts of glass beads to the suspension. The lysates were clarified by centrifugation, the protein concentration was determined, and the volume was adapted accordingly. For the IP, 20 µl of Twin-strep bead resin (Iba lifescience) was added and the samples were incubated at 4 °C for 20 minutes on a shaker. The supernatant was removed in spin columns and the beads were washed five times with buffer. After elution of proteins from the beads in 100 µl buffer BXT (Iba lifescience), samples were denatured and reduced with SDC (10 µl, 20%) and 10 mM DTT at 60 °C for 10 minutes and subsequently alkylated with 20 mM IAA at room temperature for 30 minutes. The samples were digested with trypsin (1:50 ratio to protein) at 37 °C overnight. To remove SDC, TFA (10%) was added to a final concentration of 1%. Samples were cleared and the supernatants were desalted using spin columns (Pierce).

Sample quality control for MS analysis

Sample amount and quality was determined by HPLC-UV using a Dionex UltiMate 3000 HPLC RSLC nanosystem with a PepSwift Monolithic RSLC column (0.2 x 5 mm, Thermo Fisher Scientific) at 60 °C. Peptides were separated using a 20 minutes 2-90% elution gradient of buffer B (80% ACN, 20% H_2O, 0.1% TFA).

Label free quantification mass spectrometry

LC-MS/MS analysis was performed on a Dionex UltiMate 3000 HPLC RSLC nanosystem using an Acclaim PepMap C-18 precolumn (0.3 x 5 mm, Thermo Fisher Scientific) and an Acclaim PepMap C-18 column (50 cm x 75 µm, Thermo Fisher Scientific) coupled to a Q Exactive HF-X hybrid quadrupole-Orbitrap mass spectrometer (Thermo Fisher Scientific) or a Orbitrap Exploris 480 (Thermo Fisher Scientific). Measurements using FAIMS on the Orbitrap Exploris 480 were performed at CV -45 V and CV -60 V. Peptides were separated using a 180 min linear gradient of 2-35% buffer B (80% ACN, 20% H_2O, 0.1% FA) at a flow rate of 230 nL/min. MS1 spectra were generated in a 380-1,650 *m/z* mass range at a 120,000 orbitrap resolution, AGC target of 3 x 10^6, with a maximum injection time of 50 ms. The top 10 precursors were selected for MS2 analysis using a 0.7 *m/z* quadrupole precursor isolation window, allowing charge states 2-4 and a dynamic precursor exclusion of 30 s. The orbitrap was operated at 45,000 resolution with an AGC of 1 x 10^5 and a NCE of 35% at a maximum injection time of 250 ms.

LFQ-MS and IP-MS data analysis

MS raw data were analyzed using MaxQuant (1.6.17.0) and Proteome Discoverer 2.3 (PD 2.3.0.523, Thermo) and the search was performed against a database of the *M. smegmatis* 2019 Uniprot Reference Proteome with contaminants added. The database search allowed tryptic peptides (≥ seven amino acids) with two missed cleavages at a precursor mass tolerance of 5 ppm and 0.02 Da MS2 tolerance. Static alkylation of cysteine and variable oxidation of methionine was considered. Match between runs and LFQ was enabled (MQ only) and a 1% false discovery rate cutoff was applied at PSM and protein level. In Proteome Discoverer the search engine MS Amanda[55] was used, the Percolator[65] was used for peptide scoring and filtering and protein quantification was performed using the in-house tool IMP-apQuant (https://ms.imp.ac.at/index.php?action=apQuant).

Statistical analysis of PD results as well as data normalization were performed in Perseus 1.6.[54] The samples were first filtered on high confidence FDR level and then normalized by their mean sum. Additionally, contaminants were removed, rows are filtered based on minimal values of 70% and missing values were replaced based on normal distribution.

Statistical analysis of MQ results as well as data normalization was performed in R using the in-house built LaTeX script Cassiopeia (https://github.com/moritzmadern/Cassiopeia_LFQ). Data were filtered for contaminants, for protein groups with less than two razor and unique peptides and for missing valid values in raw intensities with a cutoff of less than three valid values in at least one group. The remaining missing values were imputed from normal distribution. All mass spectrometry proteomics data in this manuscript have been deposited to the ProteomeXchange Consortium (http://proteomecentral.proteomexchange.org) via the PRIDE partner repository[66] with the dataset identifiers PXD037231, PXD037232, PXD037234 and PXD037235.

Parallel reaction monitoring (PRM) analysis

LC-MS/MS analysis was performed on a Dionex UltiMate 3000 HPLC RSLC nanosystem using an Acclaim PepMap C-18 precolumn (0.3 x 5 mm, Thermo Fisher Scientific) and an Acclaim PepMap C-18 column (50 cm x 75 µm, Thermo Fisher Scientific) coupled to a Q Exactive HF-X hybrid quadrupole-Orbitrap mass spectrometer (Thermo Fisher Scientific). Peptides were separated using a 180 min linear gradient of 2-35% buffer B (80% ACN, 20% H_2O, 0.1% FA) at a flow rate of 230 nL/min. MS1 spectra were recorded before every target cycle in a 375-1,500 *m/z* mass range at a 30,000 orbitrap resolution, AGC target of 3 x 10^6, with a maximum injection time of 60 ms. MS2 spectra were generated for targets from the isolation list using a loop count of 10. A 0.7 *m/z* quadrupole precursor isolation window was used, at 30,000 orbitrap resolution with an AGC of 2 x 10^5 and a NCE of 35% at a maximum injection time of 200 ms. For absolute quantification, heavy peptides (JPT) were included in the isolation list.

PRM data analysis

A peptide search was performed in Skyline against a database containing ClpC1, ClpC2 and ClpC3 together with three housekeeping proteins. Tryptic peptides ($\geq$ seven amino acids) were considered, with one missed cleavage and a precursor and MS2 mass tolerance of 10 ppm using the PRM acquisition method. Static alkylation of cysteine and variable oxidation of methionine was considered. For absolute quantification, a C-terminal $^{13}C(6)^{15}N(4)$ label was included. For the analysis, the top three MS2 ions were selected for all proteins and the "total area fragment" was normalized to the "average sum total area fragment" of the housekeeping proteins. For interpretation of absolute quantification, a ratio between light and heavy peptides was calculated. PRM data has been uploaded to the PanoramaWeb[67] repository (https://panoramaweb.org /iBzWpn.url; PXD037198).

M. tuberculosis samples for MS analysis

Cells of *Mtb* H37Rv WT and Δ*clpC2* mutant were grown in 20 ml supplemented Middlebrook 7H9 medium to a final $OD_{600\ nm}$ of 1. Cells were then treated with 7.8 μM HBPs or an equal volume of DMSO as solvent control and incubated for 48 h at 37 °C. Subsequently, cells were centrifuged at 4 °C and washed twice with PBS (137 mM NaCl; 2.7 mM KCl; 10 mM Na_2HPO_4; 1.8 mM KH_2PO_4; pH 7.4). Cells were resuspended in 750 μL of PBS and lysed by bead-beating in a TissueLyser LT (Qiagen) using 100-μm silica zirconium beads (50 Hz; 15 min). Afterwards, an appropriate volume of 4x lysis buffer (4% (w/v) SDS, 40 mM TCEP, 160 mM CAM, 200 mM HEPES) was added to the cells and incubated for 10 min at 95 °C. After centrifugation, the cleared supernatant was collected and used as protein lysate. To remove viable bacteria and ensure safety, the protein lysates were sterile filtered twice through a bacteria-tight 0.2 μM cellulose acetate filter.

Pull-down assays in *M. tuberculosis*

Freshly prepared *M. tuberculosis* H37Rv lysate as described above was divided into samples containing a total amount of 400 μg protein in 499 μL PBS. To each sample, 1 μL of either DMSO or the respective probes (1 mM) were added and the samples were incubated for one hour while shaking (1250 rpm, 30 min at 4 °C, followed by 30 min at room temperature). Pierce™ Avidin Agarose beads (Thermo Fisher Scientific) were equilibrated in PBS and 100 μL of a slurry suspension was added to each sample (approx. 50 μL bead volume). For proper binding of the biotin probes, the samples were incubated for one hour while shaking (1250 rpm) at room temperature. Subsequently, the beads were washed three times with PBS or in case of the competition control group with 20 μM CycloA_D9-containing PBS. An additional washing step was performed with PBS to eliminate most of the competitor. The beads were taken up in 100 μL 6 M urea in 50 mM NH_4HCO_3 (ABC) buffer, containing 20 mM DTT. After one hour of incubation, 40 mM IAA was added for alkylation of proteins and the samples were incubated for one further hour. To inactivate unreacted IAA, an equivalent amount of DTT was added and the urea concentration was reduced to 1 M by diluting the samples with 50 mM ABC buffer. For digestion, 1 μg of Trypsin (Promega) was added to each sample followed by incubation for 13 hours shaking at 37 °C. The peptide solution was acidified to 1% formic acid (FA; Fisher Chemical) and separated from the beads. The beads were washed with 1% FA in 50 mM ABC buffer and the peptide solutions were combined for further processing. To eliminate any residual beads, samples were passed through equilibrated glass microfiber tips (pore size: 1.2 μm, thickness: 0.26 mm, two disks per tip; GE Healthcare, 1822-024). Peptides were desalted on home-made C_{18} StageTips as described before.[68] For analysis, the samples were dissolved in 10 μL of 0.1% FA in water and 4 μL peptide solution was loaded on a fused silica capillary column with integrated 10 μm PicoFrit emitter with a length of 460 mm and an inner diameter of 75 μm (New Objectives PF360-75-10-N-5), self-packed with Reprosil-Pur 120 C18-AQ material (1.9 μm particles with 100 Å pore size, Dr. Maisch). The gradient was generated by an EASYnLC 1200 liquid chromatography (Thermo Fisher Scientific), using 0.1% FA in water (solvent A) and 0.1% FA with 20% water in ACN (solvent B). Peptides were separated using a 105 min gradient at a flow rate of 300 nL/mL at 50 °C. Peptides were ionized using a Nanospray Flex ion source (Thermo Fisher scientific) and MS acquisition was performed in an Orbitrap Fusion Lumos mass spectrometer (Thermo Fisher Scientific). MS1 spectra were recorded in a 375-1,800 *m/z* mass range at a 120,000 Orbitrap resolution, with standard AGC target settings at 50 ms maximum injection time. Data dependent MS2 spectra were generated using a loop cycle of three seconds with a dynamic exclusion duration of 30 seconds. A 1.2 *m/z* quadrupole precursor isolation window was used, at rapid ion trap scan rate with 300% of normalized AGC target and stepped HCD fragmentation (20, 30, 45%) with automated maximum injection time settings.

Whole cell MS from *M. tuberculosis*

Whole proteome samples were prepared following a modified SP3 protocol.[64] To this end, 15 to 20 μg of protein extract prepared as described above were treated with benzonase (40 mU/μL, EMD Millipore, 71206) for 30 min at 37 °C, followed by protein alkylation with 10 mM IAA for another 30 min at room temperature. An equal mixture of hydrophilic (Cytiva) and hydrophobic Sera-Mag SpeedBeads (Cytiva) was equilibrated to water and the beads were added to the samples to a concentration of 1 μg of particles per microliter of sample. Protein binding was induced by adding a similar volume of ethanol to the suspension followed by subsequent incubation for 30 min while shaking (1500 rpm) at room temperature. The beads were collected on a magnetic stand and washed three times with 180 μL of 80% ethanol to eliminate detergents and salts. Digestion was started by adding 100 μL of 25 mM ABC buffer containing 0.6 μg trypsin and 0.6 μg LysC. Disaggregation of the particles was promoted by sonicating the samples in a heated water bath (35-37 °C) in the first 5 min of the digestion reaction. After incubation for another 16 hours at 37 °C while shaking (1500 rpm), the beads were collected on a magnetic stand and the supernatant containing the tryptic peptides was separated from the beads. The particles were then washed with 25 mM ABC buffer and the combined peptide solutions were acidified

to a final concentration of 2% TFA. To eliminate any residual particles, samples were centrifuged at 21,000 g for 2 min and desalted on homemade C_{18} StageTips as described before.[68] Dry peptides were dissolved in 15 μL of 0.1% FA in water and peptide concentration was adjusted to 200 ng/μL. For analysis, 500 ng of peptides were loaded on a fused silica capillary column with integrated 5 μm PicoFrit emitter with a length of 410 mm and inner diameter of 75 μm (ESI Source Solutions PTC3-75-50-SP), self-packed with Kinetex XB-C18 material (1.7 μm core shell with 100 Å pore size, Phenomenex). The gradient was generated by an EASYnLC 1200 liquid chromatography (Thermo Fisher Scientific), using 0.1% FA in water (solvent A) and 0.1% FA with 20% water in ACN (solvent B). Peptides were separated using a 105 min gradient at a flow rate of 350 nL/mL at 50 °C. Peptides were ionized using a Nanospray Flex ion source (Thermo Fisher scientific) and MS acquisition was performed in an Orbitrap Fusion Lumos mass spectrometer (Thermo Fisher Scientific). MS1 spectra were recorded in a 375-1,800 *m/z* mass range at a 240,000 Orbitrap resolution, with standard AGC target settings and an automatic maximum injection time. Data dependent MS2 spectra were generated using a loop cycle of three seconds with a dynamic exclusion duration of 20 seconds. A 1.2 *m/z* quadrupole precursor isolation window was used, at rapid ion trap scan rate with 300% of normalized AGC target and stepped HCD fragmentation (20, 30, 45%) with automated maximum injection time settings. *M. tuberculosis* mass spectrometry proteomics data has been deposited to the ProteomeXchange Consortium via the PRIDE partner repository with the dataset identifiers PXD037712 and PXD037730.

Minimum inhibitory concentration (MIC) assay

Minimum inhibitory concentration testing in *M. smegmatis* was performed using the same agar-based assay as performed in Morreale et al.[26] In brief, a dilution series of each compound is prepared in 96-well plates, followed by adding agar (+ additives if applicable) to each well. Subsequent spotting of equal amounts of exponentially growing cells in each well foregoes the incubation of the plates at 37 °C. The optical readout after a few days allows for semiquantitative analysis of the minimum inhibitory concentration which prevents cell growth. For experiments with overexpression strains, the agar is supplemented with 0.1% Acetamide and 100 μg/ml Hygromycin to continue the expression of the respective gene during plate incubation. In this case, the overexpression is already induced during liquid cultivation.

Dose response curves in *M. tuberculosis*

Minimum inhibitory concentration of compounds in *Mtb* was quantified by dose response curves using the resazurin microplate assay as described previously.[69] In short, a two-fold serial dilution of tested compounds has been prepared in a polystyrene U-bottom 96-well plate (Greiner) to reflect a dose-response curve ranging from 100 μM to 0.048 μM final concentrations. Equal amounts of exponentially growing cells ($OD_{600\ nm} \leq 1$, diluted to 1 x 10^6 CFU/ml) were then added into each well to a total volume of 100 μl and cultivated for five days at 37 °C (5% CO_2, 80% humidity). Subsequently, 10 μl resazurin solution (100 μg/ml, Sigma Aldrich) was added into each well and incubated overnight. Cells were fixed at room temperature for 30 min after the addition of 10% (v/v) formalin, and growth was quantified based on fluorescence using a microplate reader (TECAN) (excitation: 540 nm, emission: 590 nm). Relative growth was calculated with respect to the DMSO solvent control (= 100%) and uninoculated wells (= 0%). Experiments were performed in triplicates. MIC_{50} values were calculated using GraphPad Prism 7 software.

Checkerboard assay

The Checkerboard analysis was used to evaluate compound susceptibility in presence of additional stressors. The experimental procedure was performed in a MIC or dose response curve assay as described above. For combinations with heat stress in *M. smegmatis*, a simultaneous increase in temperature in the first dimension was combined with reducing compound concentrations in the second dimension in a way that the final plates, already containing compound dilution series as well as cells, were incubated for the respective time at elevated temperatures and subsequently transferred to 37 °C until colonies were grown. Kanamycin was used as control. For dose response curves to simulate low ATP levels, *Mtb* H37Rv was exposed to increasing bedaquiline concentrations and HBPs or Rifampicin.

Kill curve assay

To enable monitoring of cell viability upon stress or compound incubation, exponentially growing liquid cell cultures were incubated with the respective compound in 1% DMSO or exposed to the physical stress over a time of 72 h, respectively. Every few hours, equal amounts of cells (10^3 and 10^4 CFU/ml) were plated in quadruplicates onto 7H10 agar. After incubation at 37 °C for two days, colonies were counted and CFU/ml were calculated and plotted as mean ± SD, normalized to the respective control cultures if applicable.

Minimum inhibitory time (MIT) assays

Minimum inhibitory time testing combines kill curve assays with an optically easier readout. Exponentially growing liquid cultures were exposed to the respective stressor and incubated over time. In our case, flasks were transferred to 53 °C for five hours. Starting with a control before flasks were transferred (t0) as well as after each timepoint (t1 = 1 h, t2 = 2 h, t5 = 5 h), equal amounts of cells were plated onto 7H10 agar. Precisely, a dilution series starting with 5 μl of 1x10^6 cells, followed by three serial 1:10 dilutions, thereby encompassing 5 μl of 1x10^5, 1x10^4, and 1x10^3 cells, respectively, was spotted onto the plate. The plates were then incubated at 37 °C for two days and growth performance is optically compared between the spots.

Resistance screens and WGS in *M. tuberculosis*

Spontaneous single-step resistant mutants were isolated by plating each approximately 6×10^7cells of *Mtb* H37Rv on solid media containing either 12.5 μM HBP6 or 9.4 μM HBP7, respectively. After six weeks, four colonies were isolated and subjected to MIC assays with 1:2 serial dilutions of both compounds. Rifampicin and Ethambutol were used as reference antibiotics in equally generated dose response curves of all clones. For whole genome sequencing (WGS), genomic DNA samples isolated from the mutants were quantified by photometric measurement using a NanoDrop One device (Thermo Fisher Scientific Inc.) and quality measured by capillary electrophoresis using the Fragment Analyzer and the 'High Sensitivity genomic DNA Assay' (Agilent Technologies, Inc.). Library preparation was performed according to manufacturer's protocol using TruePrep DNA Library Prep Kit V2 for Illumina (1ng) (Vazyme Biotech Co.; Ltd). Libraries were normalized to 4 nM and pooled and subsequently sequenced on a MiSeq system (Illumina Inc) with a read setup of 2x250 bp. The reads were assembled and mapped to the reference genome using the CLC Genomics Workbench (Qiagen), using *Mtb* H37RvMA as a reference (GenBank accession GCA_000751615.1).[44] Mean depth of coverage ranged from 73x – 121x. Genetic alterations observed during whole-genome resequencing analyses of spontaneous HBP6- or HBP7-resistant *Mycobacterium tuberculosis* H37Rv mutants were named as followed: HBP6 #1, #2, #3: SNP t→g at nucleotide 238 out of 2547 bp, causing amino acid substitution F80V in *clpC1* and frame shift, deletion -g at nucleotide 60 out of 6336 bp in *mas*; HBP7 #1: SNP t→c at nucleotide 83 out of 2547 bp, causing amino acid substitution I28T in *clpC1*.

Chemical Synthesis of Ecu**

2-CTC resin (1.33 mmol/g) was swelled in 5 vol% iPr$_2$NEt/CH_2Cl_2 (0.015 M) and shaken for 20 min. The solvent was discharged and the resin washed with CH_2Cl_2 (x 5). The resin was treated with the Fmoc-Gly-OH (4 eq. in regards to predicted resin loading) and iPr$_2$NEt (8 eq.) in CH_2Cl_2 (0.05 M) and shaken at room temperature for 16 h. The coupling solution was discharged and washed with CH_2Cl_2 (x 5), DMF (x 5) and CH_2Cl_2 (x 5). The resin was treated with a capping solution of 17:2:1 (v/v/v) CH_2Cl_2/iPr$_2$NEt/MeOH and shaken at room temperature for 30 min. The capping solution was discharged and the resin washed with CH_2Cl_2 (x 5) and DMF (x 5). The resin-bound peptide was treated with a solution of 10 vol% piperidine/DMF (2 x 3 min). The deprotection solution was discharged and collected and the resin washed with DMF (x 5), CH_2Cl_2 (x 5) and DMF (x 5). The combined deprotection solutions were made up to 25 mL using 10 vol% piperidine/DMF and diluted 1:100 with 10 vol% piperidine/DMF. The amount of peptide loaded to resin was determined by measurement of the UV absorbance at λ = 301 nm of the diluted deprotection solution. The resin-bound peptide was treated with a solution of a Fmoc-L-Trp(Boc)-OH acid (4 eq.) and subjected to HATU coupling conditions: HATU (4 eq.), iPr$_2$NEt (8 eq.) in DMF (0.1 M in regards to loaded peptide) and shaken for 2 h at room temperature. The coupling solution was discharged and the resin washed with DMF (x 5), CH_2Cl_2 (x 5) and DMF (x 5). The resin-bound peptide was next Fmoc-deprotected: the resin was treated with a solution of 10 vol% piperidine/DMF (2 x 3 min). The deprotection solution was discharged and the resin washed with DMF (x 5), CH_2Cl_2 (x 5) and DMF (x 5). The resin-bound peptide was treated with a solution of 2-nitrobenzenesulfonyl chloride (4 eq.) and 2,4,6-trimethylpyridine (10 eq.) in NMP (0.1 M in regards to loaded peptide) and shaken at room temperature for 20 min. The protection solution was discharged and the resin washed with DMF (x 5), CH_2Cl_2 (x 5) and THF (x 10). The resin-bound peptide was treated with a solution of PPh_3 (5 eq.) and anhydrous MeOH (10 eq.) in anhydrous THF (0.2 M in regards to loaded peptide). The resin was shaken at room temperature for 1 min at which point an additional solution of DIAD (5 eq.) in THF (0.2 M in regards to loaded peptide) was sucked into the fritted syringe. The resin was shaken for 15 min, the solution was discharged and the resin washed with DMF (x 5), CH_2Cl_2 (x 5) and DMF (x 5). The resin-bound peptide was treated with a solution of DBU (5 eq.) and 2-mercaptoethanol (10 eq.) in NMP (0.1 M in regards to loaded peptide) (2 x 5 min). The deprotection solution was discharged and the resin washed with DMF (x 5), CH_2Cl_2 (x 5) and DMF (x 5). The resin-bound peptide was treated with a solution of a Fmoc-*N*-Me-L-Ala-OH (2 eq.) and subjected to HATU/HOAt coupling conditions: HATU (2 eq.), HOAt (4eq.) and iPr$_2$NEt (4 eq.) in DMF (0.1 M in regards to resin loading) and shaken for 8 h at room temperature. The coupling solution was discharged and the resin washed with DMF (x 5), CH_2Cl_2 (x 5) and DMF (x 5). The resin was then Fmoc-deprotected (using the aforementioned protocol). The resin-bound peptide was treated with a solution of Fmoc-L-Val-OH (4 eq.) according to the HATU/HOAt coupling conditions used previously. Fmoc-L-Val-OH was coupled three times to ensure complete coupling. Coupling progress was monitored *via* UPLC-MS. The resin-bound peptide was then Fmoc-deprotected and treated with a solution of Fmoc-*N*-Me-L-Leu-OH according to the HATU coupling conditions mentioned previously. The resin bound peptide was then Fmoc-deprotected. The resin-bound peptide was washed with CH_2Cl_2 (x 10) and then treated with a solution of 30 vol% HFIP/ CH_2Cl_2 (3 x 20 min). The cleavage solution was discharged, collected and concentrated under a stream of N_2 and dried *in vacuo*. The crude protected linear peptide was purified by preparative RP-HPLC using a Sunfire OBD 5 μm 19 x 150 mm (C18) column using a gradient of 30 – 45% ACN in H_2O (0.1% TFA) over 30 min at a flow rate of 25 mL/min. The peptide was lyophilized to yield the protected linear peptide as a trifluoroacetate salt (86 mg, 82% over 12 steps from resin loading, average of 98% per step). The peptide (1.09 mg, 1.36 μmol) was deprotected with iPr$_3$SiH:TFA:CH_2Cl_2 (2:49:49, v/v/v, 1 mL) and stirred at room temperature for 1 h, then concentrated under a stream of N_2. The peptide was redissolved in ACN:H_2O (1:1, v/v, 1 mL) with 1 drop of AcOH and stirred at room temperature overnight. The peptide was then lyophilized to give the pure deprotected linear peptide (1.0 mg, 82% over 13 steps from resin loading). The peptide was re-lyophilized five times with 0.25 M HCl to convert the trifluoroacetate salt to the hydrochloride salt. NMR data are provided in Data S1**C**.

Chemical Synthesis of dCym-JQ1 (SRG-II-19F)

Reactions were monitored by LC/MS (*Shimadzu Prominence-i LC-2030*, column: *Phenomenex Onyx C18*, 50 x 4.6 mm, *Shimadzu LCMS-2020*, (ESI)). Flash chromatography (reversed phase) was conducted with a *Büchi Reveleris PREP* on *Büchi Flashpure Select C18* cartridges, H_2O/ACN gradient). The compounds were dried by lyophilization from ACN/H_2O overnight. ^{1}H and ^{13}C spectra were recorded with Bruker AV 500 [500 MHz (^{1}H), 126 MHz (^{13}C)] spectrometers in $CDCl_3$ at 298 K. Chemical shifts are reported in ppm relative to $Si(CH_3)_4$. The signals of residual $CHCl_3$ in $CDCl_3$ ($\delta(^{1}H, CHCl_3)$ = 7.26 ppm, $\delta(^{13}C, CDCl_3)$ = 77.16 ppm) were used as the internal standard. Multiplicities are reported as (singlet), d (doublet), t (triplet), q (quartet) and m (multiplet). High resolution mass spectra were recorded on a *Bruker MAXIS 4G* UHR-TOF (ESI). **[6-propargyl]-dCym** and **JQ1-PEG$_4$-N$_3$** were prepared as described.[26,29]

2-((*S*)-4-(4-Chlorophenyl)-2,3,9-trimethyl-6*H*-thieno[3,2-f][1,2,4]triazolo[4,3-a][1,4]diazepin-6-yl)-N-(14-(4-(((3-(((2*S*,5*S*,8*S*,11*S*,14*S*,17*S*,20*S*)-5-((*R*)-3-hydroxy-2-methylpropyl)-17-isobutyl-14,20-diisopropyl-11-((*R*)-methoxy(phenyl)methyl)-4,8,16-trimethyl-3,6,9,12,15,18,21-heptaoxo-1,4,7,10,13,16,19-heptaazacyclohenicosan-2-yl)methyl)-1*H*-indol-1-yl)methyl)-1*H*-1,2,3-triazol-1-yl)-3,6,9,12-tetraoxatetradecyl)acetamide (dCym-JQ1 / SRG-II-19F)

In a 1.5 mL vial, **[6-propargyl]-dCym** (18.0 mg, 19.0 μmol] and **JQ1-PEG$_4$-N$_3$** (14.8 mg, 23.0 μmol) were dissolved in a mixture of t-BuOH (190 μL) and H_2O (190 μL). 1 M $CuSO_4$ (9.56 μL, 9.56 μmol) and freshly prepared 1 M sodium ascorbate (11.0 μL, 11.0 μmol) solutions were added, the vial was flushed with Argon and stirred at RT for 12 h. Then, the reaction mixture was concentrated *in vacuo* and the residue was purified by flash chromatography (H2O/ACN 70:30 – 5:95). After lyophilization, dCym-JQ1 (28.0 mg, 180 μmol, 84%, purity >95%) was obtained as a white amorphous solid. See Data S1**C** for synthesis scheme, NMR and HPLC data.

Synthesis of pArg-JQ1 (BI01826025)

The synthesis of the pArg-JQ1 basically followed previously published synthesis protocols.[26] In brief, commercially available (+)-JQ1 (150 mg, 0.33 mmol) was dissolved in 4 M HCl in dioxane (5 mL) and stirred for 1 h at RT. The solvent was removed under reduced pressure and the residue was redissolved in DCM (10 mL). Mono-Boc-protected diaminoethyl ether (102 mg, 1.5 eq., 0.50 mmol), HOBt monohydrate (77 mg, 1.5 eq., 0.50 mmol), DIC (77 μL,1.5 eq., 0.50 mmol) and triethyl amine (218 μL, 4.7 eq., 1.57 mmol) were added and the resulting mixture was stirred for 16 h at rt. 5% aq. $NaHCO_3$ solution (10 mL) was added, the organic phase was separated, dried over $MgSO_4$ and evaporated to dryness, resulting in 174 mg (0.30 mmol, 90%) of a white solid that was used in the next step without further purification. The residue was redissolved in 4 M HCl in dioxane (5 mL) and stirred for 4 h at RT. The solvent was removed under reduced pressure and the residue was redissolved in DCM (5 mL). Fmoc-pArg(Tce)$_2$-OH (325 mg, 1.5 eq., 0.44 mmol), HOBt monohydrate (97 mg, 2.1 eq., 0.63 mmol), DIC (196 μL, 4 eq., 1.26 mmol) and triethyl amine (217 μL, 5.2 eq., 1.56 mmol) were dissolved in DCM (20 mL) and added to the first mixture. The resulting solution was stirred for 16 h at RT. 5% aq. $NaHCO_3$ solution (10 mL) was added, the organic phase was separated, dried over $MgSO_4$ and evaporated to dryness. The resulting crude product was dissolved in DCM (6 mL) and diethyl amine (4 mL) were added. This mixture was stirred for 4 h at RT. 5% aq. $NaHCO_3$ solution (10 mL) was added, the organic phase was separated, dried over $MgSO_4$ and evaporated to dryness. The resulting residue was redissolved in DCM (5 mL) and acetic anhydride (54 μL, 1.9 eq., 0.57 mmol) and triethylamine (158 μL, 3.8 eq., 1.14 mmol) was added. The resulting reaction mixture was stirred for 1 h at RT. The mixture was evaporated to dryness and the resulting residue was purified by column chromatography (stationary phase: C18-RP, eluent gradient (acetonitrile: water, 0.1% formic acid): 50:50 → 60:40 → 70:30→ 100:0). Product containing fractions were pooled and evaporated to dryness, resulting in 76 mg (0.074 mmol,23%) of the desired Tce-protected intermediate (TLC (DCM/MeOH 9:1 + 0.5 % formic acid): R_f 0.4). The Tce-protected intermediate (128 mg, 0.11 mmol) was then dissolved in a mixture of NH_4HCO_3 buffer (100 mM, pH 9, 5 mL) and ethanol (5 mL). 10% Pd on carbon (55 mg) was added as a hydrogenation catalyst and the mixture was flushed with argon, then with H_2 for 5 h at RT. The mixture was again flushed with argon, the catalyst was filtered off and the solution was reduced to dryness. The remaining residue was purified by HPLC (C18-RP, gradient: 10% → 60% acetonitrile in water containing 0.1% ammonia). Product containing fractions were pooled and lyophilized, thereby yielding 11 mg (0.0144 mmol, 13%) of the desired pArg-JQ1. See Data S1C for synthesis scheme, NMR and HPLC data.

QUANTIFICATION AND STATISTICAL ANALYSIS

Reported SPR K_D values represent the average ± SD of the indicated number of independent measurements. Volcano plots for proteomics (whole proteome and IP-MS) analysis show the fold-change (log_2) in protein abundance in comparison to control treatment, plotted against *P* value ($-log_{10}$) (two-tailed Student's T-test; triplicate analysis). All MIC data are represented as mean ± SD of the indicated replicate experiments. All degradation assay data are represented as mean ± SD of the indicated replicate experiments. Indicated replicates always refer to independent biological replicates and datasets.

CellPress
OPEN ACCESS

Supplemental figures

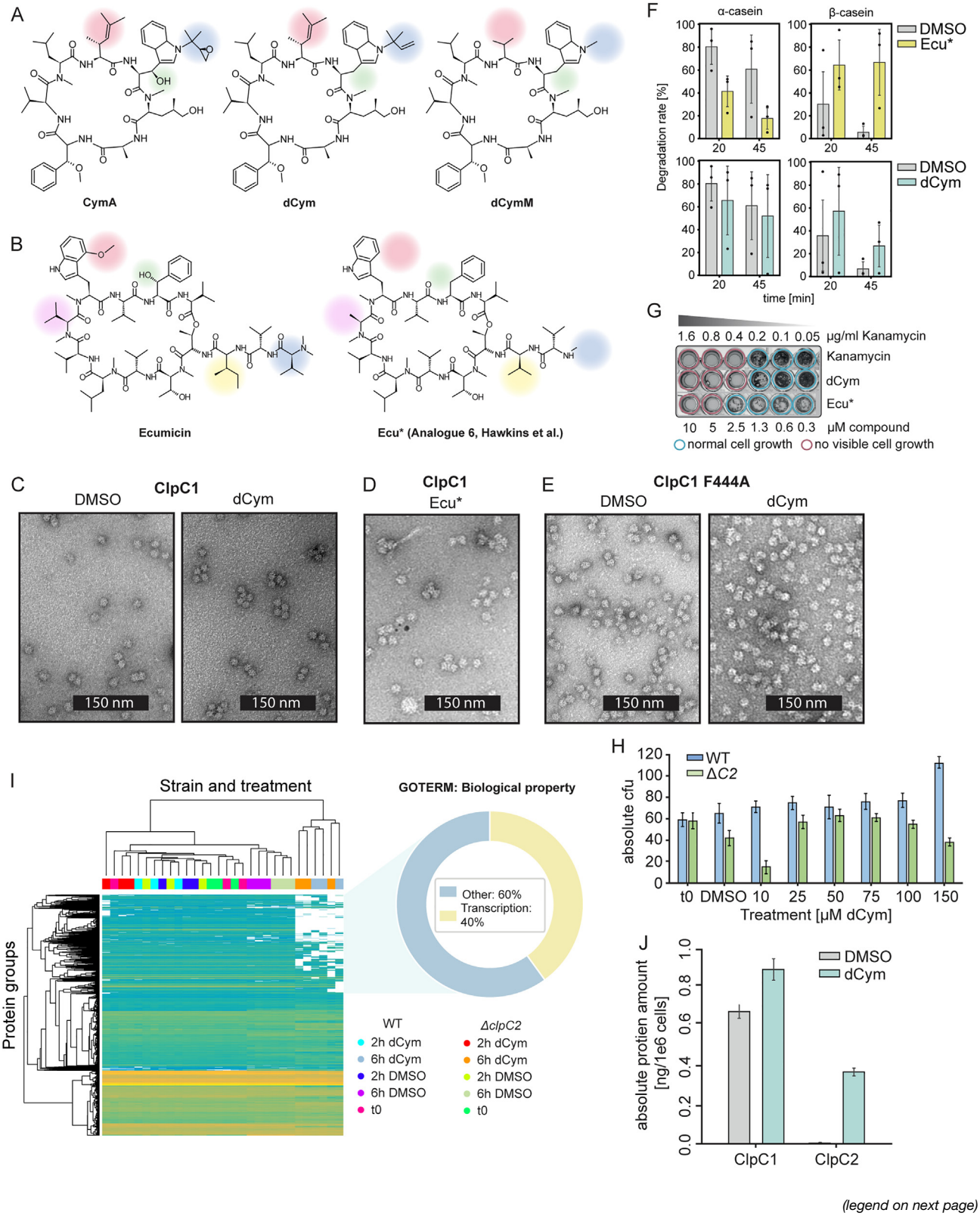

(legend on next page)

Figure S1. Cyclomarin A and ecumicin derivatives are effective in *M. smegmatis*, related to Figure 1

(A) Structures of natural cyclomarin A (CymA) and derived compounds used in this study. The colors represent the residue positions where the natural compound has been changed.[19,26,46]

(B) Structure of ecumicin and its derivatives used in this study. The colors represent the residue positions where the natural compound has been changed.

(C–E) Negative-stained EM images of ClpC1 and ClpC1^{F444A} mutants with and without bound antibiotics.

(F) Substrate degradation of two model substrates, β-casein and α-casein, by ClpC1P1P2 with or without dCym or Ecu* (Quantification represents mean ± SD, n = 3).

(G) Minimum inhibitory concentration (MIC) assay testing appropriate concentrations of dCym and Ecu* for treatment of wild-type cells. n ≥ 10 independent biological replicates.

(H) Kill curve assay comparing wild type and *ΔclpC2* after treatment with increasing dCym concentrations. 2-h incubation allowed the use of 150-μM dCym without significant growth effects. Reduced viability of *ΔclpC2* with 10 μM dCym likely presents an experimental outlier, due to occasional stronger biofilm formation of stressed *ΔclpC2* cells. The presented dataset shows mean ± SD of three technical replicates.

(I) Quantitative proteomics of *Msm* treated with 150 μM dCym for 2 or 6 h, respectively. The heatmap plots identified protein groups across the different samples. Color coding for different strains and conditions according to the legend. The zoomed in data in circle shows the distribution of the GO terms no longer quantifiable in mutant samples. n = 3 independent biological replicates.

(J) Absolute quantification of ClpC1 and ClpC2 levels. ClpC2 significantly increases upon dCym treatment. Results are mean ± SD from three independent biological replicates. CFU, colony-forming unit.

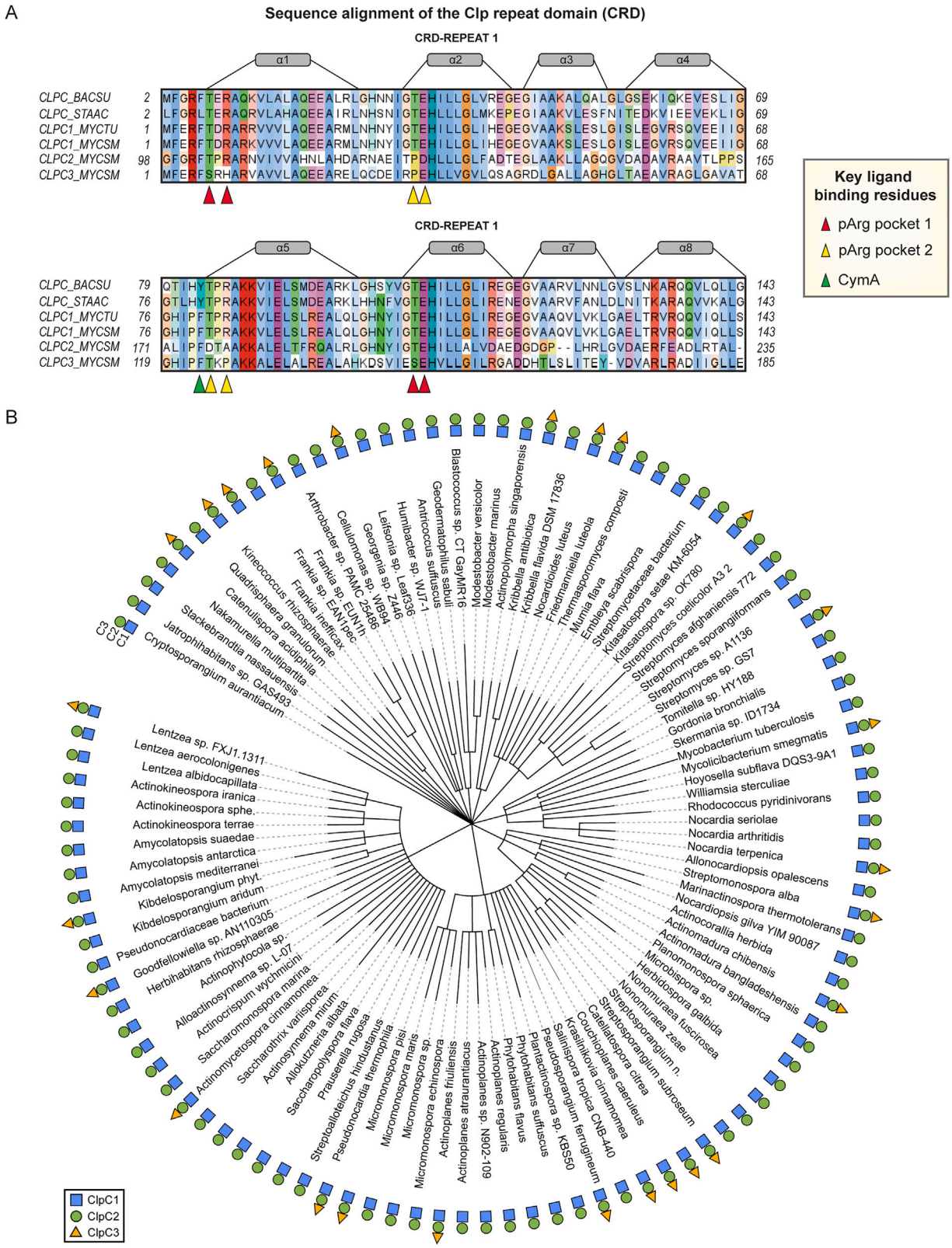

(legend on next page)

Figure S2. Conservation of Clp proteins, related to Figure 2

(A) Sequence alignment showing the conservation of key binding residues within the CRD of Clp proteins.

(B) Taxonomic tree showing conservation of ClpC1, ClpC2, and ClpC3 in representatives of actinobacterial species. BACSU, *Bacillus subtilis*; STAAC, *Staphylococcus aureus* COL; MYCSM, *Mycolicibacterium smegmatis* mc^2 155; MYCTU, *Mycobacterium tuberculosis* H37Rv.

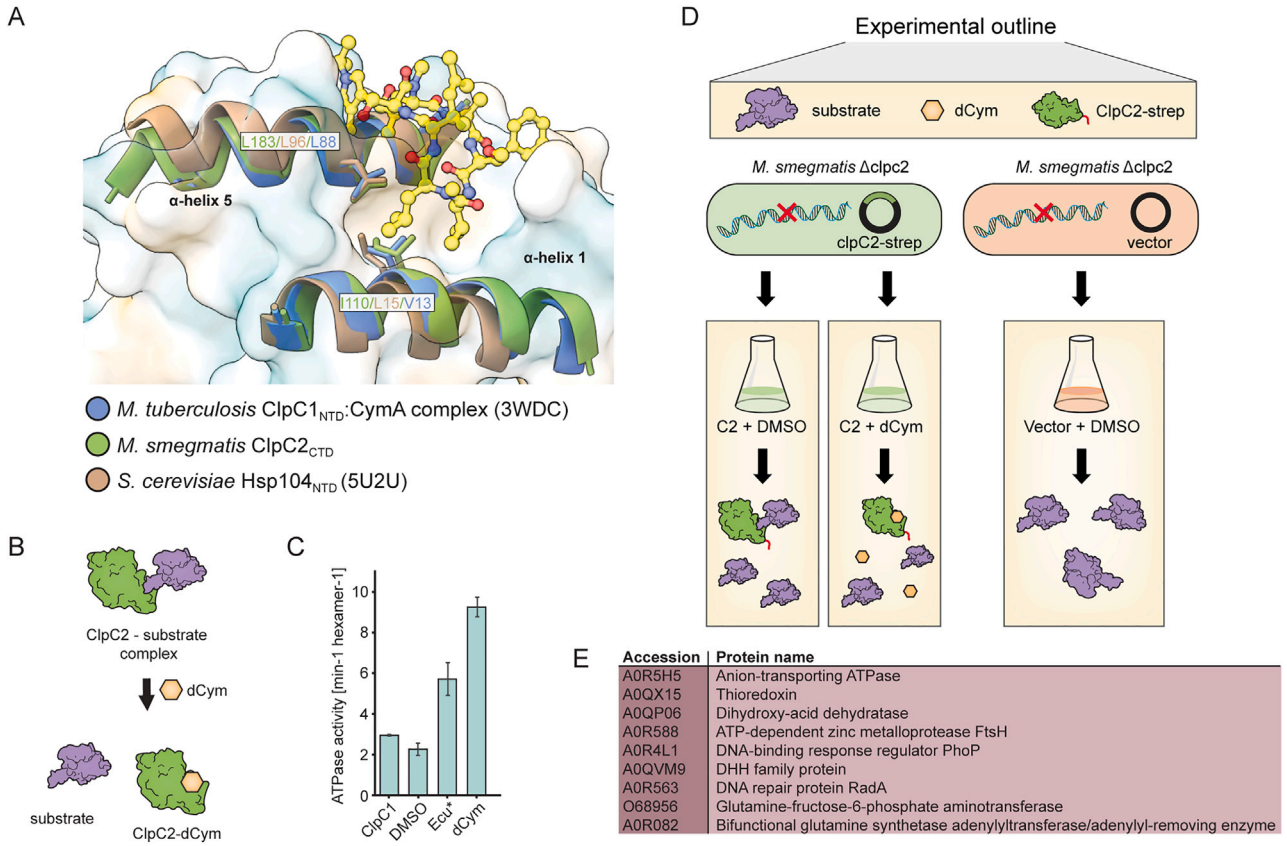

E

Accession	Protein name
A0R5H5	Anion-transporting ATPase
A0QX15	Thioredoxin
A0QP06	Dihydroxy-acid dehydratase
A0R588	ATP-dependent zinc metalloprotease FtsH
A0R4L1	DNA-binding response regulator PhoP
A0QVM9	DHH family protein
A0R563	DNA repair protein RadA
O68956	Glutamine-fructose-6-phosphate aminotransferase
A0R082	Bifunctional glutamine synthetase adenylyltransferase/adenylyl-removing enzyme

Figure S3. Interactions between dCym and ClpC2, related to Figure 3

(A) Conserved hydrophobic residues implicated in substrate binding to Hsp104 (PDB 5U2U) are blocked by CymA in the $ClpC1_{NTD}$.

(B) Schematic model illustrating competition between dCym and substrate for the same binding site.

(C) ATPase activity assay shows increasing ATPase activity upon compound treatment. Results are mean ± SD from three independent biological replicates.

(D) Experimental outline describing pull-down experiments with ClpC2. *Msm ΔclpC2* overexpresses plasmidic $ClpC2^{twinstrep}$. Interaction partners of ClpC2 are analyzed by IP-MS (left, green). After dCym incubation, interaction partners of ClpC2 compete with dCym for the binding (middle, green). Empty vector was used as control (right, orange).

(E) Among the most abundant hits in ClpC2 pull-down, nine proteins are homologs to proteins previously identified in ClpC1 degradome analysis in *Mtb*.

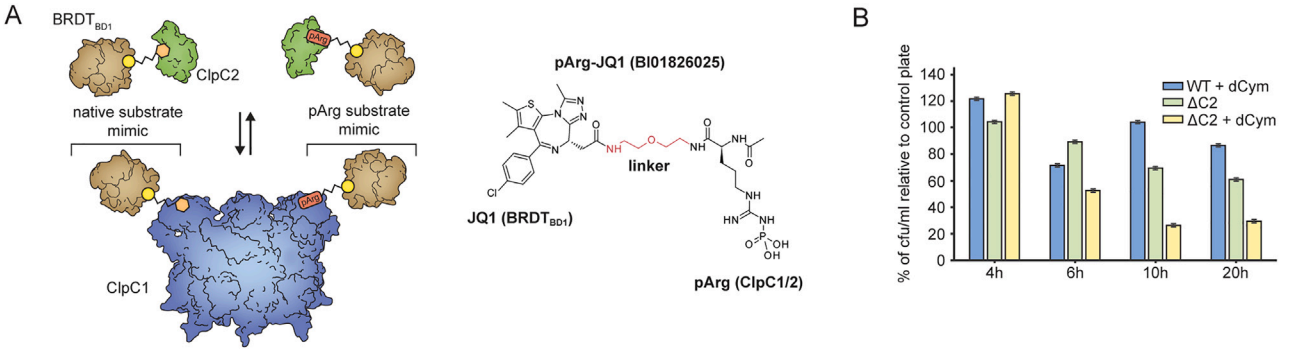

Figure S4. Role of ClpC2 during induced degradation and cell survival, related to Figure 4

(A) ClpC2 (green) competes for binding BRDT$_{BD1}$ model substrates (brown) by either pArg-JQ1 or dCym-JQ1, representing two distinct degradation signals (on the right: structure of the pArg-JQ1).

(B) Kill curve assay, monitoring survival of *Msm* wild type and *ΔclpC2* mutant over time upon dCym treatment. After incubation with 150 μM dCym, equal amounts of cells were plated onto 7H10 agar and CFU/mL were counted to compare cell viability. Deletion of *clpC2* significantly decreases survival. Results are mean ± SD from three independent biological replicates. CFU, colony-forming unit.

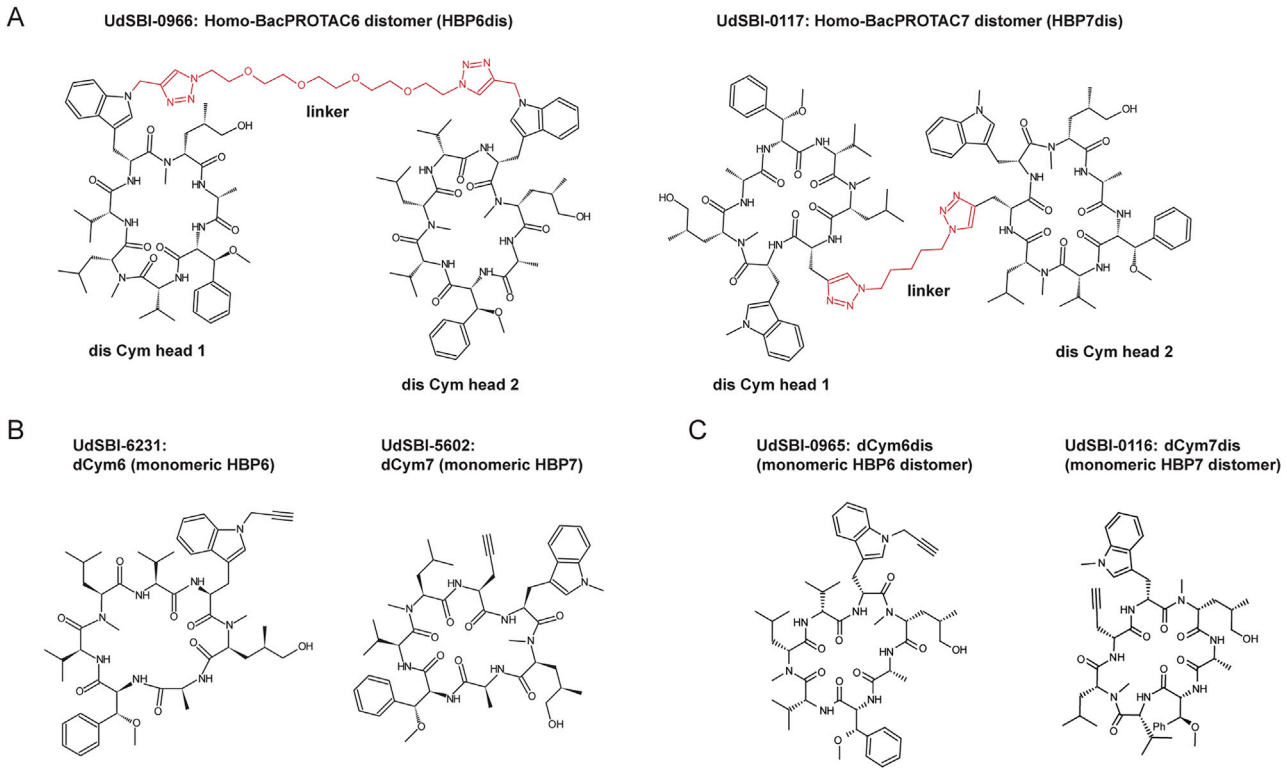

Figure S5. Homo-BacPROTAC distomers and monomers, related to Figure 5

Compound structures for inactive Homo-BacPROTAC6 distomer (A) and Homo-BacPROTAC7 distomer (B) active monomers of Homo-BacPROTAC6 and Homo-BacPROTAC7 (C) inactive monomers of the distomers of Homo-BacPROTAC6 and Homo-BacPROTAC7.

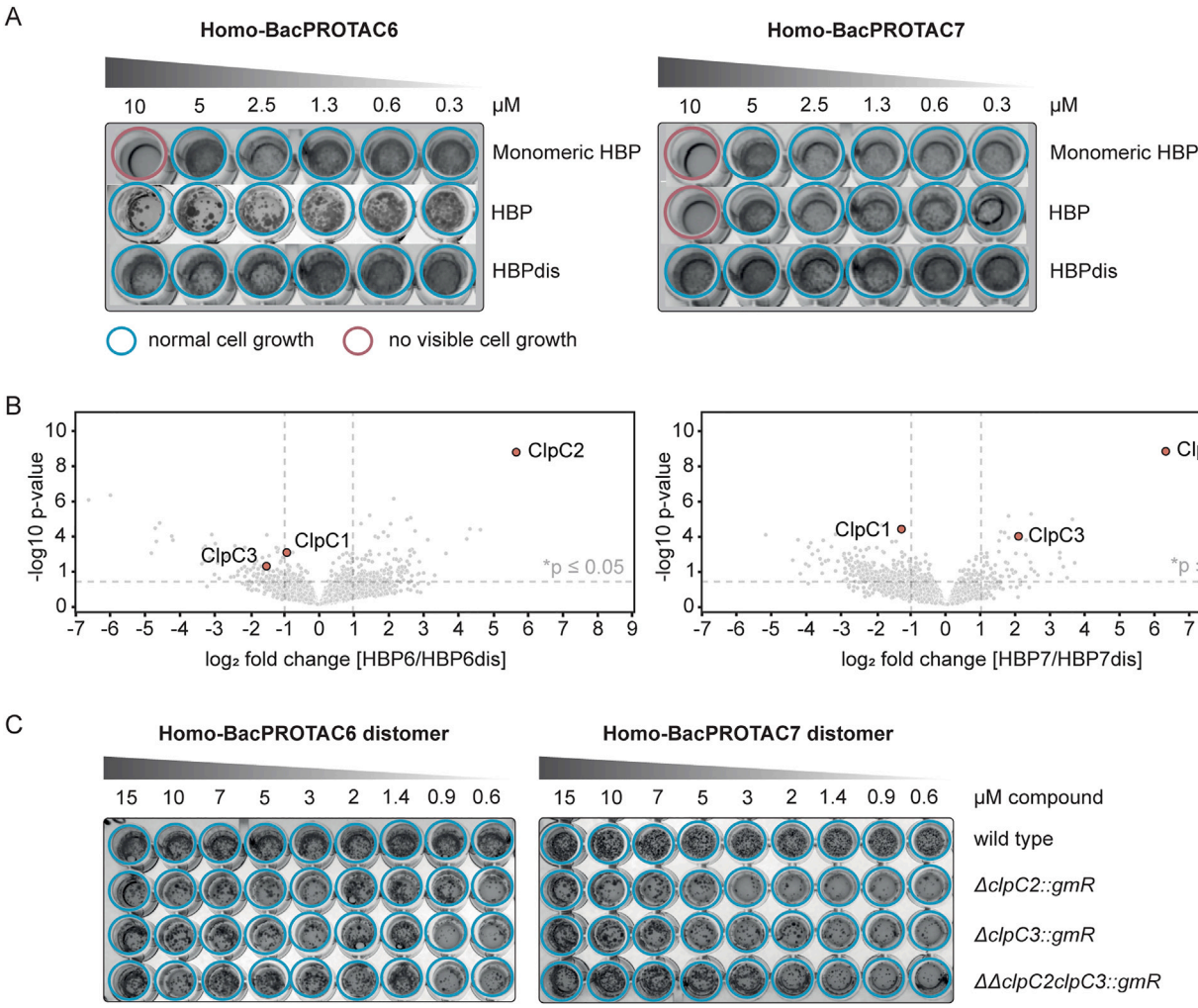

Figure S6. Controls for incubation with Homo-BacPROTACs in *Msm*, related to Figure 6

(A) MIC assays exposing wild-type cells to either active compounds, inactive distomer or the corresponding monomers (+ linker attached). 1:2 dilution series. Activity of both monomeric and dimeric compound is comparable and low for both Homo-BacPROTACs. No MIC has been observed for distomers. n ≥ 6 independent biological replicates.

(B) Quantitative proteomics of Homo-BacPROTACs HBP6 and HBP7 treated *Msm* cells after 24 h, normalized to incubation with inactive distomers (HBP6dis, HBP7dis). n = 3 independent biological replicates.

(C) MIC assays comparing wild type and mutants incubated with corresponding distomers of Homo-BacPROTACs (1:3 dilution series). No MIC can be observed for either distomer in any of the strains. n = 6 independent biological replicates. gmR, gentamicin resistance cassette introduced instead of *clpC2*/*clpC3*.

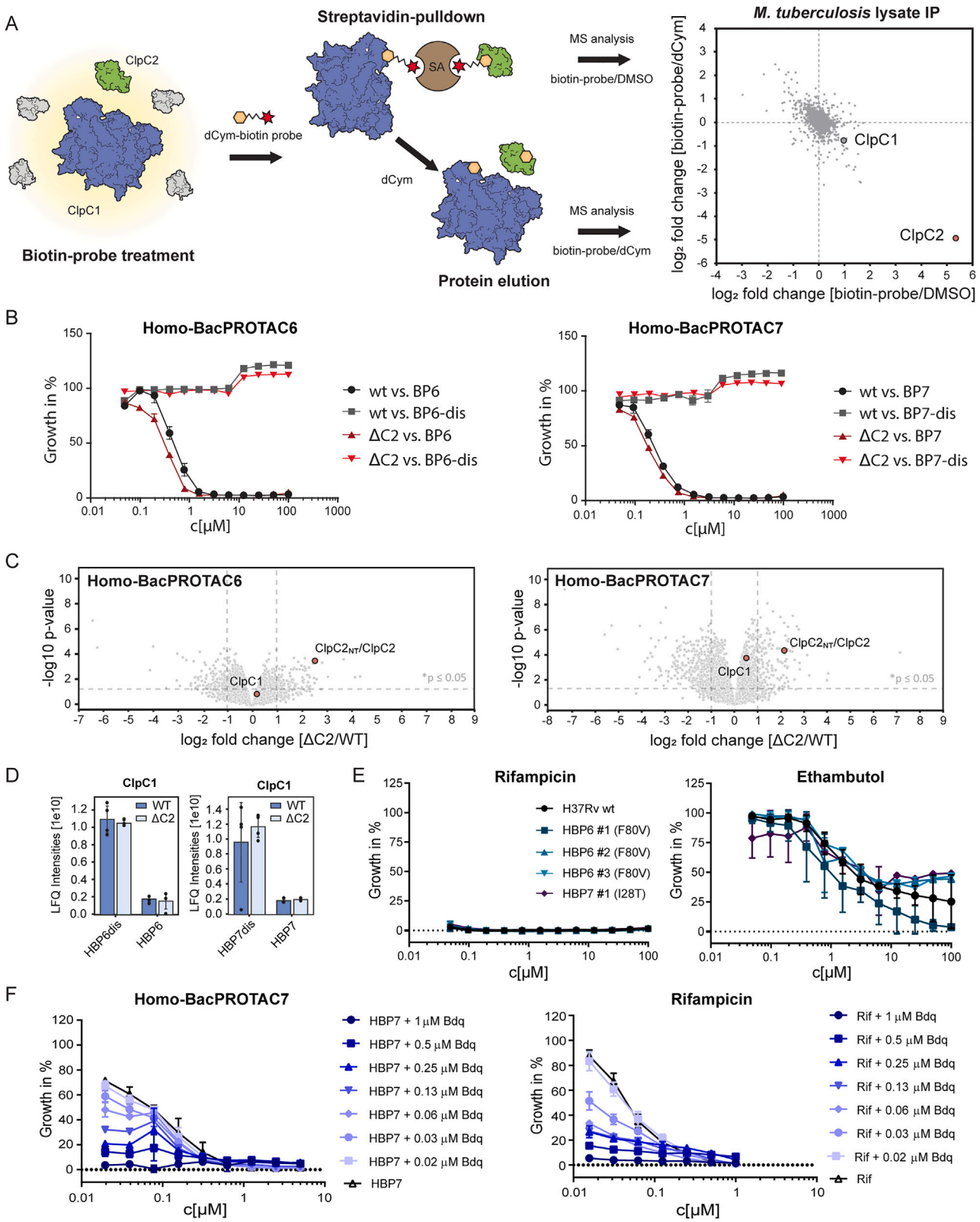

(legend on next page)

Figure S7. IP-MS and activity analysis of HBP variants in healthy and ATP-reduced *M. tuberculosis*, related to Figure 7

(A) Pull-down assays in *Mtb* identified ClpC1 and ClpC2 as major interaction partners of dCym. The experimental outline is shown on the left. n = 3 independent biological replicates.

(B) Dose response curves comparing WT *Mtb* with the *ΔclpC2* mutant upon incubation with HBP6 or HBP7. The mutant is slightly more sensitive than the WT, consistent with the safeguarding function of ClpC2. Distomers do not inhibit cell growth. Results are mean ± SD from three independent biological replicates.

(C) Quantitative proteomics of *Mtb* WT and *ΔclpC2* cells, with the latter expressing a truncated 21-aa ClpC2 peptide ($ClpC2_{NT}$). While ClpC1 is reduced to similar levels in treated WT and *ΔclpC2* bacteria, levels of ClpC2 (WT) and $ClpC2_{NT}$ (*ΔclpC2*) are strikingly different. This difference likely reflects induced degradation of ClpC2 in WT cells, whereas the $ClpC2_{NT}$ peptide is inaccessible to HBP-mediated degradation. Quantification shows mean ± SD from three independent biological replicates.

(D) LFQ intensities comparing ClpC1 degradation induced by HBP6 and HBP7 and their corresponding distomers. Results are mean ± SD from three independent biological replicates.

(E) MIC assays comparing susceptibility of four *Mtb* spontaneous single-step resistant mutants against reference antibiotics. All mutants showed unaltered susceptibility toward rifampicin and ethambutol, ruling out unspecific resistance mechanisms. The additionally affected *mas* gene is involved in phthiocerol dimycocerosate (PDIM) synthesis. Since mutations causing PDIM loss are known to occur very frequently during *in vitro* culturing of *Mtb* strains[39] this second-site mutation is likely irrelevant for the observed resistance phenotype. Results are mean ± SD from measurements done in triplicates.

(F) Activity of HBP7 against *Mtb* cells at low ATP levels determined in a *Mtb* checkerboard assay. HBP7 retains activity in cells that have been co-treated with the ATP synthase inhibitor bedaquiline, similar to a rifampicin control. Results are mean ± SD from measurements done in triplicates. PDIM, phthiocerol dimycocerosate; SRM, spontaneous single-step resistant mutant.